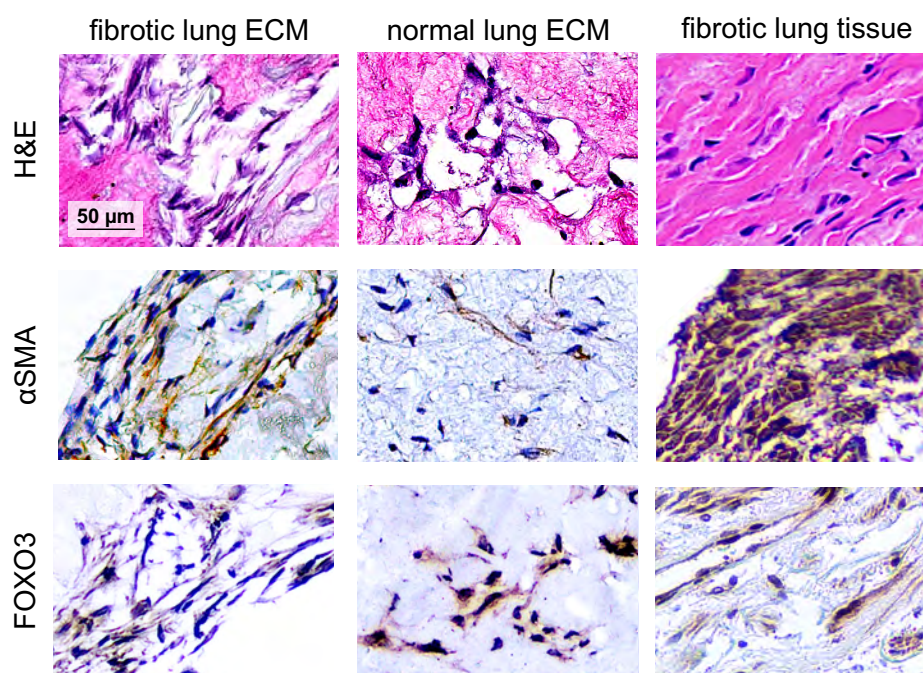


# Fibrotic human lung extracellular matrix as a disease-specific substrate for 3D *in-vitro* models of pulmonary fibrosis



Igal Germanguz<sup>†</sup>, Evelyn Aranda<sup>†</sup>, Jennifer C. Xiong, Natalia Kissel,

Alexandra Nichols, Eddie Gadee, John D. O'Neill\*

Xylyx Bio, Inc.  
760 Parkside Avenue  
Brooklyn, New York 11226, USA

<sup>†</sup> Authors contributed equally

\* Correspondence: John D. O'Neill, Email: [john@xylyxbio.com](mailto:john@xylyxbio.com)

1 **Fibrotic human lung extracellular matrix as a disease-specific substrate for 3D *in-vitro***  
2 **models of pulmonary fibrosis**

3

4 Igal Germanguz<sup>1†</sup>, Evelyn Aranda<sup>1†</sup>, Jennifer C. Xiong<sup>1</sup>, Natalia Kissel<sup>1</sup>, Alexandra Nichols<sup>1</sup>, Eddie  
5 Gadee<sup>1</sup>, John D. O'Neill<sup>1\*</sup>

6

7 <sup>1</sup> Xylyx Bio, Inc., 760 Parkside Avenue, Brooklyn, New York 11226, USA

8 <sup>†</sup> Authors contributed equally

9 \* Correspondence: John D. O'Neill, Email: [john@xylyxbio.com](mailto:john@xylyxbio.com)

10

11 **ABSTRACT**

12 Idiopathic pulmonary fibrosis (IPF) is an irreversible and uniformly fatal lung disease marked by  
13 destruction and scarring of the lung parenchyma and progressive loss of respiratory function. IPF  
14 affects nearly 3 million people worldwide, and annual mortality in the US alone exceeds 40,000.  
15 Nintedanib and pirfenidone, the only drugs approved for the treatment of IPF, slow progression  
16 but do not cure the disease. Consequently, there is a pressing need for effective treatments  
17 beside lung transplantation. Unfortunately, predictive models of IPF are not available,  
18 underscoring the critical need for physiologically relevant *in-vitro* substrates that enable  
19 quantitative and mechanistic studies of human IPF. Here we report the development and  
20 characterization of a human pulmonary fibrosis-specific cell culture substrate comprised of intact  
21 fibrotic lung extracellular matrix that recapitulates the human IPF disease environment *in vitro*.  
22 We document the activation and disease-specific phenotype of human lung fibroblasts cultured  
23 in the IPF disease-specific substrate, and establish feasibility of testing antifibrotic agents using  
24 this substrate. Altogether, our results demonstrate the applicability of this fibrosis-specific  
25 substrate for 3D *in-vitro* models of IPF and cell-based assays in early-stage drug discovery.

- 26 **Keywords:** 3D cell culture, drug testing, extracellular matrix, idiopathic pulmonary fibrosis, *in-*  
27 *vitro* models, lung disease, lung fibroblasts, scaffolds

## 28 INTRODUCTION

29 Idiopathic pulmonary fibrosis (IPF) is a chronic interstitial lung disease that primarily affects older  
30 adults and is associated with dysregulation of pulmonary fibroblasts, extensive remodeling and  
31 deposition of extracellular matrix, and progressive loss of respiratory function.<sup>1-3</sup> Incidence and  
32 prevalence appear to be increasing worldwide with aging populations and improved diagnostics.<sup>4</sup>  
33 Every year more than 50,000 new patients are diagnosed with IPF<sup>5</sup> – an incidence comparable  
34 to those of liver, stomach, testicular, or cervical cancers.<sup>6</sup> After diagnosis, median survival is only  
35 3 – 4 years, and annual mortality exceeds 40,000.<sup>7</sup> The etiology of IPF remains unknown, but risk  
36 factors include smoking, environmental exposures, chronic viral infections, gastroesophageal  
37 reflux, lung injury, and genetic predispositions.<sup>4,8</sup> Nintedanib and pirfenidone, the only drugs  
38 approved to treat IPF, attenuate disease progression but do not prevent decline,<sup>1,4,9</sup> necessitating  
39 the development of new drugs that can effectively treat IPF.

40  
41 A major obstacle to developing effective treatments for IPF is the lack of predictive animal and *in-*  
42 *vitro* models of IPF. Animal models of pulmonary fibrosis are well-established in rodents<sup>10-12</sup> but  
43 present fibrosis that resolves over time rather than the progressive, non-resolving fibrotic process  
44 characteristic of IPF in humans.<sup>3,13</sup> Furthermore, there are no robust or widely adopted *in-vitro*  
45 models of IPF to enable predictive basic and translational studies.<sup>14</sup> Consequently, an *in-vitro*  
46 model of IPF that emulates human pathophysiology could enable critical new insights into the  
47 natural history and pathological mechanisms of IPF, and guide therapeutic development.

48  
49 Current *in-vitro* models of IPF have limited physiologic relevance because they fail to recapitulate  
50 the complex biochemical, structural, and mechanical environment of fibrotic human lungs. In  
51 fibrosis, the extracellular matrix (ECM) has different biochemical composition, stores more  
52 fibrogenic growth factors, and has altered structure and biomechanics compared to normal  
53 ECM,<sup>15-17</sup> and the direct influence of growth factors<sup>18,19</sup> and increased matrix stiffness<sup>20</sup> on

54 myofibroblast differentiation has been previously demonstrated. Altogether, such matrix  
55 alterations induce a profibrotic microenvironment, activate pulmonary fibroblasts, and suggest  
56 that IPF progression is correlated with an abnormal ECM microenvironment.<sup>21</sup> As lung matrix is  
57 implicated in both lung function and fibrotic disease progression, IPF models and drug screening  
58 platforms not incorporating lung ECM lack defining components of the IPF disease environment.  
59 The most common *in-vitro* IPF drug testing platforms utilize cell culture plates coated with collagen  
60 type I and culture media supplemented with high concentrations of transforming growth factor  $\beta$   
61 (a profibrotic cytokine associated with fibrogenesis),<sup>22</sup> but no testing platforms that utilize other  
62 IPF disease-specific ECM components have been established.

63

64 An *in-vitro* cell culture substrate comprised of fibrotic human lung matrix could faithfully  
65 recapitulate the composition, structure, and mechanics of the human IPF disease environment.  
66 While removal of native cells (decellularization) from human tissues has been demonstrated in a  
67 number of tissues including lungs<sup>23-26</sup>, efforts have been primarily focused on the isolation and  
68 characterization of ECM from normal, non-diseased tissues. Reproducible, scalable methods for  
69 the production of disease-specific ECM biomaterials from diseased human tissues such as fibrotic  
70 lungs have not been robustly established. Furthermore, an *in-vitro* cell culture substrate that  
71 recapitulates the complex disease environment of human IPF tissue would be an extremely  
72 valuable tool for screening antifibrotic agents in early-stage development.

73

74 In this study, we investigated the feasibility of developing a cell culture substrate from fibrotic  
75 human lung tissue for 3D *in-vitro* models of human pulmonary fibrosis. Our hypothesis was that  
76 normal human lung fibroblasts would display a disease-specific phenotype *in vitro* in the presence  
77 of fibrotic lung extracellular matrix. We implemented a 'physiomimetic approach' to develop  
78 disease-specific IPF cell culture substrates (scaffolds) comprised of lung extracellular matrix  
79 derived from human IPF tissues (**Fig. 1**). Our goal was to develop a human fibrotic lung ECM

## Physiomimetic approach for development of disease-specific cell culture substrates

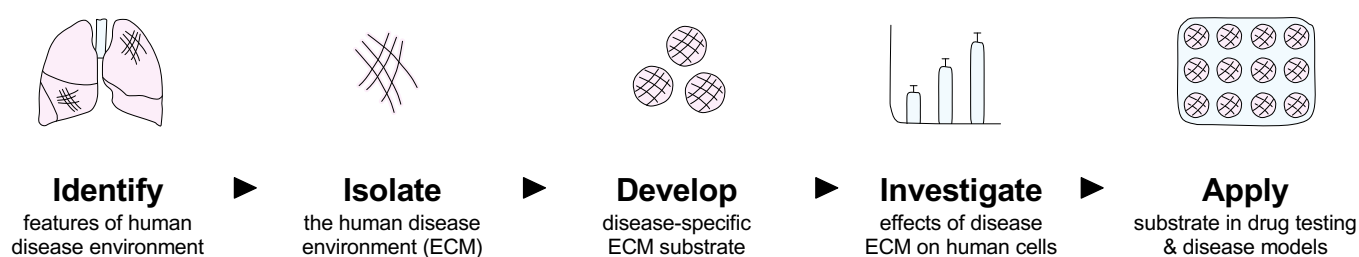


**Figure 1 | Overview of physiomimetic approach.** Our development of IPF disease-specific cell culture substrates is guided by a physiomimetic approach that aims to identify and isolate the human disease environment, then develop and investigate disease-specific ECM substrates *in vitro* utilizing disease-relevant human cell types (e.g., pulmonary fibroblasts) whose phenotype can be directly compared against diseased human IPF lung specimens prior to application in IPF disease models and antifibrotic drug testing.

80 biomaterial for use as a 3D cell culture substrate for predictive *in-vitro* models of IPF that could  
81 reduce dependence on animal models while enabling physiologically relevant results. Such  
82 disease-specific cell culture substrates could radically improve the physiological relevance of *in-*  
83 *vitro* models of IPF and antifibrotic drug screening platforms, and accelerate development of safe  
84 and effective IPF treatments.

85

## 86 **MATERIALS & METHODS**

87

88 **Procurement of human lung tissues.** Acceptance criteria for donors of normal and IPF lungs  
89 were established prior to initiation of studies. Normal lung donors had no history, diagnosis, or  
90 evidence of: smoking, aspiration pneumonia, asthma, chronic obstructive pulmonary disease,  
91 cystic fibrosis, emphysema, interstitial lung disease, or lung cancer. IPF donors required  
92 diagnosis of idiopathic pulmonary fibrosis confirmed by a lung transplant pathologist. All IPF  
93 donors had end-stage disease and were recipients of lung transplants. Normal human lungs ( $n =$   
94 3) not acceptable for use in transplantation were procured under a protocol approved by the  
95 Institutional Review Board at the International Institute for the Advancement of Medicine.  
96 Diseased human lungs ( $n = 3$ ) designated as surgical waste were procured under protocols  
97 approved by the Institutional Review Boards at Vanderbilt University Medical Center and State  
98 University of New York (SUNY) Downstate Medical Center. Lungs were procured in standard  
99 fashion, flushed with cold organ preservation solution, transported on ice, and made available  
100 without identifiers. In this study, to minimize variability, lung tissues from right middle and right  
101 lower lobes were utilized.

102

103 **Characterization of lung donors.** Lung donor characteristics were tabulated from deidentified  
104 summaries provided by the United Network of Organ Sharing (UNOS) under approved protocols  
105 and in compliance with all applicable regulations.

106 **Sampling of lung tissues.** Tissue samples were collected from medial, lateral, and peripheral  
107 regions of right middle lobes (2 samples per region), for a total of 6 regional samples per right  
108 middle lobe, and 18 regional samples each for IPF and normal lungs.

109

110 **Preparation of lung matrix scaffolds.** Upon receipt, lungs were rinsed with cold sterile saline.  
111 Native lung tissue samples were collected for histologic analyses, then lung tissues were stored  
112 at  $-80^{\circ}\text{C}$ . At the time of use, lung tissues were processed under sterile conditions with a  
113 proprietary combination of chemicals, enzymes, and surfactants to remove cellular components  
114 and isolate normal and fibrotic lung extracellular matrix. Matrix scaffolds (diameter: 7 mm,  
115 thickness: 1 mm) were prepared under sterile conditions for experimental use. For all assays,  
116 three tissue samples or matrix scaffolds were randomly selected from each lung and evaluated in  
117 triplicate.

118

119 **Histologic analyses of lung tissues and scaffolds.** Lung tissue samples were fixed in cold  
120 phosphate-buffered 4% paraformaldehyde for 24 hours, embedded in paraffin, and sectioned at  
121 5 or 10  $\mu\text{m}$  thickness. Three sections (medial, lateral, peripheral) from all normal and fibrotic lungs  
122 were stained with hematoxylin and eosin, trichrome, Verhoeff–Van Gieson, Alcian blue, and  
123 pentachrome, and examined under light microscopy. Representative images were obtained using  
124 a fluorescence microscope (FSX100, Olympus).

125

126 **Histopathologic characterization of lung tissues.** All lung sections were subjected to blinded  
127 review by a lung transplant pathologist. Slides were randomized, arbitrarily numbered, and  
128 delivered without reference to the pathologist, who reviewed and assigned fibrosis scores to all  
129 regions in 5 high-power fields according to a standard pulmonary fibrosis scoring rubric<sup>27</sup> to  
130 quantify the extent of architectural disruption and fibrosis (**Supplementary Fig. 1C**). Fibrosis  
131 scores from each high-power field were averaged to obtain an average fibrosis score for each



132 region of lung. To quantitatively assess the severity and distribution of fibrosis, a grid with unit  
133 length 250  $\mu\text{m}$  was overlaid onto each high-power field (20 $\times$ ) image, and regions corresponding  
134 to various classifications of fibrosis were outlined (**Supplementary Fig. 1F**). Each region was  
135 assigned a calculated relative percent area of the high-power field using the grid. Each fibrosis  
136 score was weighted according to percent area, and average fibrosis scores for each high-power  
137 field were calculated based on the weighted average of all regional fibrosis scores in each high-  
138 power field. Fibrosis scores were then averaged across 5 high-power fields per region, with four  
139 regions evaluated per lobe. Only regions of IPF lungs with confirmed fibrosis score  $\geq 2$  were  
140 investigated in this study (**Supplementary Fig. 1D,E,G**).

141

142 **Biochemical characterization of lung tissues and scaffolds.** To quantify collagen in lung  
143 tissues and scaffolds, samples were weighed, homogenized, and digested with pepsin (0.1 mg  
144  $\text{mL}^{-1}$ ) in 0.5M acetic acid for 12 hours at 4°C, and subjected to a collagen quantification assay  
145 (Sircol, Biocolor) according to the manufacturer's instructions. To quantify sulfated  
146 glycosaminoglycans in lung tissues and scaffolds, samples were weighed, homogenized, and  
147 digested with papain (1  $\mu\text{g mL}^{-1}$ ) for 12 hours at 60°C, and subjected to the dimethylene blue dye  
148 assay, wherein absorbance was measured at 595 nm. To quantify elastin in lung tissues and  
149 scaffolds, samples were weighed and homogenized, and soluble  $\alpha$ -elastin was extracted via  
150 three extractions with hot 0.25M oxalic acid. Samples were then subjected to an elastin  
151 quantification assay (Fastin, Biocolor) according to the manufacturer's instructions. To quantify  
152 residual DNA in matrix scaffolds, samples were subjected to a quantitative DNA assay (Quant-iT  
153 PicoGreen, Invitrogen) according to the manufacturer's instructions.

154

155 **Immunohistochemical staining.** Following de-paraffinization, sections of lung tissues and  
156 scaffolds were subjected to boiling citrate buffer (pH 6.0) for antigen retrieval, and blocked with  
157 5% normal goat serum in phosphate-buffered saline for 1 hour at room temperature. Next,

158 antibodies were diluted as necessary, applied, and incubated for 12 hours at 4°C or 4 hours at  
159 room temperature. Sections were mounted (VectaMount Permanent Mounting Medium, Vector  
160 Laboratories), and coverslips were applied. Images were obtained using a light microscope  
161 (Eclipse Ts2, Nikon). Immunohistochemical stains were performed for alpha smooth muscle actin  
162 (Cell Signaling Technology, 19245), fibrillin 2 (Sigma Life Science, HPA012853), Ki67  
163 (ThermoFisher Scientific, PA1-38032), laminin  $\gamma$ 1 (Abcam, ab233389), matrix gla protein (LS Bio,  
164 LS-B14824), and periostin (Abcam, ab14041). A list of antibodies with dilutions used is provided  
165 in **Supplementary Table 1**.

166  
167 **Quantification of immunohistochemical staining by image analysis.** Images of immuno-  
168 histochemical stains were captured using a slide scanner (P250 High Capacity Slide Scanner, 3D  
169 Histech). To quantify immunohistochemical staining, images were analyzed using an image  
170 analysis software module (DensitoQuant, Quant Center, 3D Histech), and the number of positive  
171 and negative pixels were quantified and analyzed.

172  
173 **Mass spectrometry of IPF and normal lung matrisomes.** Detailed methods are available in the  
174 Supplementary Information.

175  
176 **Quantification of growth factors.** To quantify growth factors in native lung tissues and matrix  
177 scaffolds, a multiplex growth factor array (Quantibody Human Growth Factor Array Q1; Ray  
178 Biotech) was performed and analyzed by Q-Analyzer software. To quantify growth factors  
179 secreted by human fibroblasts *in vitro*, enzyme-linked immunosorbent assays (ELISA) were  
180 performed for bFGF (R&D Systems, DFB50) and TGF $\beta$  (R&D Systems, DB100B). All samples  
181 were analyzed in triplicate.

182 **Scanning electron microscopy.** Lung matrix samples were collected, fixed in formalin for 24  
183 hours, rinsed in 70% ethanol, frozen, lyophilized, and imaged using an electron microscope  
184 (GeminiSEM 300, Zeiss) with accelerating voltage 2.5 kV.

185  
186 **Transmission electron microscopy.** Lung matrix samples were fixed with 2.5% glutaraldehyde,  
187 4% paraformaldehyde, and 0.02% picric acid in 0.1M Na-cacodylate buffer (pH 7.2). Samples  
188 were then post-fixed with 1% OsO<sub>4</sub> in Sorenson's buffer for 1 hour, dehydrated, and embedded  
189 in Lx-112 (Ladd Research Industries). Sections (thickness: 60 nm) were prepared using a PT-XL  
190 ultramicrotome, stained with uranyl acetate and lead citrate, and examined with an electron  
191 microscope (JEM-1200 EXII; JEOL). Images were captured with a digital camera (ORCA-HR;  
192 Hamamatsu Photonics) and recorded with imaging software (Image Capture Engine, AMT).

193  
194 **Mechanical testing of IPF and normal lung scaffolds.** Uniaxial tensile mechanical testing was  
195 conducted with a 10 N load cell (Model 5848, Instron), as previously described.<sup>23</sup> Lung tissues  
196 and matrix from transverse sections of the right middle lobe were randomly selected and  
197 dissected into 3 cm by 1 cm samples. A consistent orientation from right middle lobe was  
198 maintained to minimize effects of lung anisotropy on mechanical testing data. Samples were  
199 secured and mounted, and a pre-load of 0.003 N was applied. All samples were tested at the  
200 same grip-to-grip distance for consistency. Samples were kept hydrated throughout all  
201 mechanical testing with phosphate-buffered saline at room temperature. A 20% uniaxial strain  
202 was applied at a strain rate of 1% s<sup>-1</sup>, and at frequencies of 0.25, 0.50, or 0.75 Hz.

203  
204 **Cell culture.** Human lung fibroblasts (ATCC) were cultured in Dulbecco's Modified Eagle Medium  
205 (DMEM) supplemented with 10% fetal bovine serum and 1% penicillin/streptomycin under  
206 standard culture conditions with 5% CO<sub>2</sub> at 37°C.

207 **Gene expression analysis.** Total RNA was extracted (RNeasy Micro Kit, QIAGEN), and cDNA  
208 synthesis was performed using random primers (iScript Select cDNA Synthesis Kit, Bio-Rad).  
209 Quantitative real-time polymerase chain reaction (qPCR) was performed in triplicate using master  
210 mix (Brilliant III Ultra-Fast SYBR Green QPCR Master Mix, Agilent Technologies) and a real-time  
211 PCR system (AriaMax Real PCR System, Agilent Technologies). A list of primers is provided in  
212 **Supplementary Table 2.**

213

214 **Drug testing.** Normal human fibroblasts were cultured *in vitro* for 24 hours, then exposed to  
215 antifibrotic agent PF3644022 hydrate (PZ-0188, Sigma-Aldrich) at a concentration of 1  $\mu$ M for 72  
216 hours. Metabolic activity was measured using Alamar Blue reagent (DAL1025, ThermoFisher  
217 Scientific) according to the manufacturer's instructions. The reagent was added to cells in culture  
218 at 24, 48 and 72 hours, and incubated for 4 hours before readout. Absorbance was measured at  
219 570nm, with reference wavelength at 600 nm.

220

221 **Statistical analyses.** One-way ANOVA and Student's *t*-tests were performed using statistical  
222 analysis software (Prism 8, GraphPad), and  $p < 0.05$  was considered significant.

223

## 224 **RESULTS**

225

226 **Assessment of IPF and normal lungs.** Donor characteristics of IPF and normal lung tissues  
227 were analyzed to confirm that there were no significant differences in age, height, weight, body  
228 mass index, or smoking history (**Supplementary Fig. 1A,B; Supplementary Table 3**). An  
229 established numerical rubric<sup>27</sup> was used to assess the extent of histomorphologic disruption and  
230 fibrosis. Tissue sampling and histopathologic analyses are described in detail in Supplementary  
231 Information.

232 **Preparation of lung matrix scaffolds.** Native lung tissues were treated with a proprietary  
233 combination of chemicals, enzymes, and surfactants to remove cellular and nuclear components,  
234 which was confirmed by hematoxylin and eosin staining (**Fig. 2A**) and quantitative DNA assay  
235 (**Supplementary Fig. 2A**). Matrix scaffolds from all human lungs were confirmed negative for  
236 mycoplasma, bacteria, and fungi (**Supplementary Fig. 2B**), and deemed suitable for use in cell-  
237 based studies.

238

239 **IPF matrix scaffolds recapitulate disease-specific histologic features.** For histologic  
240 evaluations of IPF, representative fields corresponding to fibrosis score 3 (severe fibrosis) were  
241 selected. To visualize distributions of ECM structural components in IPF and normal lungs,  
242 histologic staining was performed on native (untreated) tissues and matrix scaffolds. H&E staining  
243 of native IPF tissues revealed severe distortion of lung structure and large areas of fibrous  
244 obliteration with minimal remaining airspace (**Fig. 2A**). By contrast, H&E staining of native normal  
245 lung tissues displayed abundant airspaces defined by thin alveolar septa and stereotypical  
246 alveolar saccular architecture. Matrix scaffolds from analogous regions of IPF and normal lungs  
247 had no discernible nuclei and displayed drastic differences in scaffold architecture consistent with  
248 fibrotic and normal native lung tissues, respectively. Trichrome staining showed dramatic  
249 deposition of collagens (blue) throughout regions of severe fibrosis (**Fig. 2B**). In IPF tissues and  
250 scaffolds, collagen fibers were observed in densely aligned bundles and in loosely disorganized  
251 networks; whereas in normal lung tissues and scaffolds, collagen was organized along alveolar  
252 septa and within the interstitium. Verhoeff–Van Gieson (VVG) elastic staining showed a notable  
253 loss of elastic fibers (black) in regions of IPF tissues and scaffolds with severe fibrosis, whereas  
254 in normal lung tissues and scaffolds elastic fibers were dispersed homogenously throughout the  
255 respiratory zone (**Fig. 2C**).

256

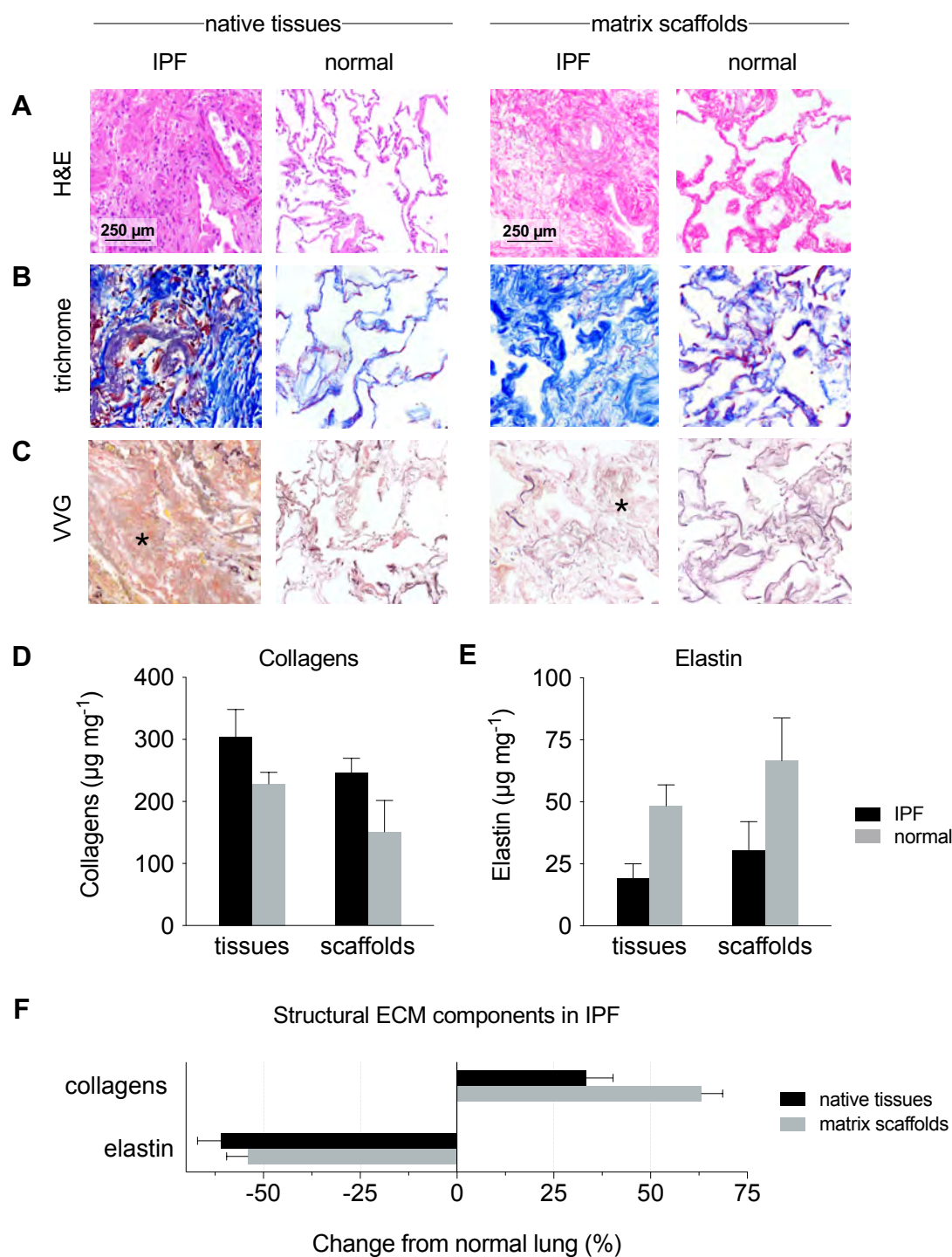
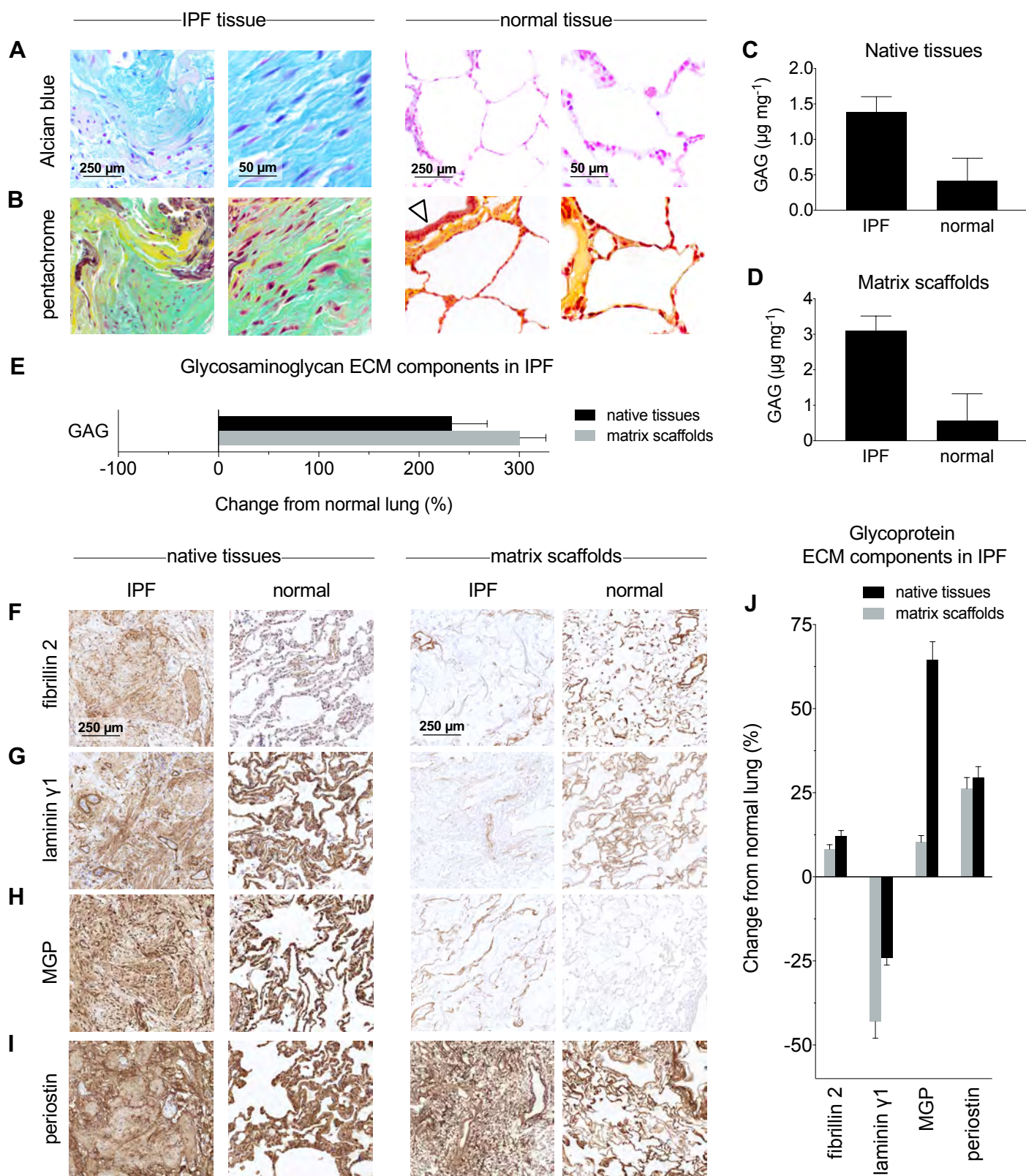


**Figure 2 | Histologic & biochemical characterization of ECM structural components in IPF and normal lung tissues and matrix scaffolds.** Representative micrographs of histologic stains: (A) hematoxylin and eosin (H&E), (B) trichrome (collagens, blue), and (C) Verhoeff–Van Gieson (VVG, elastic fibers, black) demonstrating differences in histomorphology of IPF and normal lung tissues and scaffolds. Star indicates representative region with severe fibrosis and loss of elastic fibers. Quantification of structural ECM components (D) collagens and (E) elastin by biochemical assays. (F) Changes from normal lung in structural ECM components in IPF. H&E: hematoxylin and eosin, VVG: Verhoeff–Van Gieson.

257 **IPF matrix scaffolds contain disease-specific biochemical composition.** Soluble collagens  
258 were quantified in native tissues and matrix scaffolds, and increases in collagens were measured  
259 relative to normal in IPF native tissues ( $33.3 \pm 19.2$  %) and matrix scaffolds ( $63.2 \pm 15.6$  %, **Fig.**  
260 **2D**). Consistent with the loss of elastic fibers observed in VVG elastic staining, quantification of  
261 elastin confirmed reduction in IPF native tissues ( $60.6 \pm 12.3$  %) and matrix scaffolds ( $54.1 \pm 17.2$   
262 %) relative to normal (**Fig. 2E**). Altogether, the structural ECM components in IPF demonstrated  
263 clear trends relative to normal in both native tissues and matrix scaffolds: increased collagens (33  
264 – 63%) and decreased elastin (54 – 61%; **Fig. 2F**). Alcian blue and pentachrome staining were  
265 performed to assess the extent and distribution of proteoglycans in IPF tissues, which was  
266 significantly higher in areas of moderate and severe fibrosis (scores  $\geq 2$ ) than in areas of mild  
267 fibrosis (scores  $< 2$ ) and normal lung tissues (**Fig. 3A,B**). Quantification of sulfated  
268 glycosaminoglycans (GAG) revealed that GAG components in IPF native tissues and scaffolds  
269 was 232.5 – 300.5% higher than in normal lungs (**Fig. 3C-E**), consistent with overexpression of  
270 sulfated glycosaminoglycans previously observed in fibrotic foci<sup>28</sup>. Immunohistochemical staining  
271 of IPF tissues for multiple ECM glycoproteins revealed dramatic differences from normal lung  
272 tissues in fibrillin 2, laminin  $\gamma 1$ , matrix GLA protein (MGP), and periostin (**Fig. 3F-I**). Areas with  
273 severe fibrosis (fibrosis score: 3) were characterized by pervasive overexpression of fibrillin 2,  
274 MGP, and periostin, and loss of laminin  $\gamma 1$ . Notably, changes from normal lung were consistent  
275 in native tissues and matrix scaffolds for all glycoproteins that were investigated (**Fig. 3J**).















































276  
277 Mass spectrometry was performed on IPF and normal lung matrix scaffolds to assess the IPF  
278 matrisome (**Table 1**), and revealed changes from normal lung consistent with histopathologic  
279 observations and biochemical assays. Multiple collagen types increased above 150%, including  
280 collagen types I, II, V, VI, VIII, XVI. Notably, in IPF lungs collagen types IV and XXI – the primary  
281 collagens comprising the alveolar basement membrane – decreased between 33 – 73%,  
282 consistent with the loss of basement membrane and alveolar structure associated with the





**Figure 3 | Characterization of proteoglycans and glycoproteins in IPF lung tissues and matrix scaffolds.** Representative micrographs of histologic stains: (A) Alcian blue (proteoglycans, blue) and (B) pentachrome (acidic polysaccharides, green) demonstrating differences in proteoglycans between IPF and normal lung tissues. Arrow indicates normal airway epithelium. Quantification of sulfated glycosaminoglycan ECM components in (C) native tissues and (D) matrix scaffolds. (E) Changes from normal lung in glycosaminoglycan ECM components in IPF. Immunohistochemical staining of glycoprotein ECM components in IPF: (F) fibrillin 2, (G) laminin  $\gamma$ 1, (H) matrix gla protein (MGP), (I) periostin. (J) Quantification of glycoproteins by image analysis of immunohistochemical staining using DensitoQuant software.



Protein category	Description	Change from normal (%)	
<b>Collagens</b>	type II, $\alpha$ 1 chain	5688.9	
	type XVI, $\alpha$ 1 chain	511.1	
	type I, $\alpha$ 1 chain	260.0	
	type VI, $\alpha$ 3 chain	255.6	
	type VIII, $\alpha$ 1 chain	202.3	
	type V, $\alpha$ 1 chain	196.2	
	type I, $\alpha$ 2 chain	188.2	
	type V, $\alpha$ 2 chain	164.3	
	type VI, $\alpha$ 2 chain	161.8	
	type VI, $\alpha$ 1 chain	156.4	
	type I, $\alpha$ 3 chain	139.0	
	type V, $\alpha$ 3 chain	127.4	
	type IV, $\alpha$ 2 chain	-32.9	
	type IV, $\alpha$ 1 chain	-35.7	
	type IV, $\alpha$ 3 chain	-63.5	
	type IV, $\alpha$ 5 chain	-63.7	
	type IV, $\alpha$ 4 chain	-70.2	
	type XXI, $\alpha$ 1 chain	-72.9	
	<b>Glycoproteins</b>	vitronectin	966.7
periostin		295.8	
fibulin 2		222.2	
laminin subunit $\alpha$ 5		169.1	
dermatopontin		107.7	
laminin subunit $\beta$ 2		-38.6	
laminin subunit $\gamma$ 1		-43.9	
nidogen 1		-52.8	
laminin subunit $\alpha$ 3	-60.0		
<b>Proteoglycans</b>	biglycan	633.3	
	heparan sulfate PG core protein (BM-specific)	-37.8	
<b>Elastin</b>	elastin isoform	-31.1	
<b>Matrisome secreted factors</b>	hornerin	101.4	
<b>ECM regulators</b>	metalloproteinase inhibitor 3 (TIMP3)	637.5	
	cathepsin G	500.0	
	desmoplakin	414.3	
	serum albumin precursor	278.8	
	$\alpha$ 1-antitrypsin	240	
	junction plakoglobin	202.9	
<b>Immune factors</b>	complement component C9	1422.2	
	immunoglobulin $\gamma$ 1 heavy chain	688.9	
	serum amyloid P-component	298.7	
	neutrophil defensin 3	-28.1	
<b>Keratin structural proteins</b>	type I, cytoskeletal 9	259.4	
	type I, cytoskeletal 14	170.6	
	type II, cytoskeletal 2	167.2	
	type II, cytoskeletal 5	162.4	
	type I, cytoskeletal 10	149.8	
	type II, cytoskeletal 1	145.9	

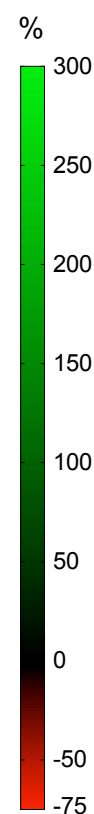


**Table 1 | Mass spectrometry summary analysis of IPF lung matrisome.** Changes from normal in the abundance of IPF lung matrisome components. PG: proteoglycan, BM: basement membrane,

283 progression of pulmonary fibrosis.<sup>29</sup> The glycoprotein vitronectin was elevated 967%, and  
284 glycoproteins fibulin 2 and periostin were both elevated above 200%. Laminin subunits  $\alpha$ 3,  $\beta$ 2,  
285  $\gamma$ 1, and nidogen 1, which are associated with the basement membrane, were all decreased in IPF  
286 lungs. Biglycan was increased by 633%, however basement membrane-specific heparan sulfate  
287 proteoglycan core protein was decreased by 38%. Elastin isoforms were also decreased by 31%,  
288 consistent with quantitative biochemical analyses. Interestingly, in IPF lungs several regulators of  
289 the extracellular matrix were also increased more than 200% above normal, including  
290 metalloproteinase inhibitor 3 (TIMP3), cathepsin G, desmoplakin, and  $\alpha$ 1-antitrypsin.

291

292 To assess changes in endogenous growth factors, a multiplex growth factor array was performed.  
293 Two growth factors were detected only in IPF native tissues and not in normal lung native tissues:  
294 transforming growth factor beta 3 (TGF- $\beta$ 3) and heparin-binding EGF-like growth factor (HB-EGF;  
295 **Supplementary Table 4**). In IPF native tissues, insulin-like growth factor binding protein 1  
296 (IGFBP-1) was 160-fold above normal, and both basic fibroblast growth factor (bFGF) and  
297 endocrine gland-derived vascular endothelial growth factor (EG-VEGF) were approximately 20-  
298 fold above normal. Brain-derived neurotrophic factor (BDNF) and growth differentiation factor 15  
299 (GDF-15, a prognostic factor for IPF<sup>30</sup>) were elevated 3-fold to 5-fold, but osteoprotegerin (OPG)  
300 was reduced by more than half. Five growth factors were detected in IPF matrix scaffolds (**Table**  
301 **2**), including IGFBP-6, whose family of carrier proteins were shown to induce production of  
302 collagen type I and fibronectin in normal primary lung fibroblasts<sup>31,32</sup>. Neurotrophin-4 (NT-4),  
303 which is elevated in explanted IPF lungs and shown to drive proliferation of primary human lung  
304 fibroblasts through TrkB-dependent and protein kinase B-dependent pathways<sup>33</sup>, was also  
305 detected in IPF matrix scaffolds.

306

307 **IPF matrix scaffolds have disease-specific structural and mechanical properties.** The gross  
308 appearance of IPF matrix scaffolds was dramatically different from the appearance of normal lung

Growth factor	Description	Concentration (pg mL <sup>-1</sup> )		Fold change from normal
		Normal scaffold	IPF scaffold	
GDF-15	Growth differentiation factor 15	0.8	14.5	+ 18.1 ▲
BDNF	Brain-derived neurotrophic factor	6.3	48.7	+ 7.7 ▲
IGFBP-6	Insulin-like growth factor binding protein 6	14.1	71.8	+ 5.1 ▲
HGF	Hepatocyte growth factor	23.8	91.0	+ 3.8 ▲
EG-VEGF	Endocrine gland-derived vascular endothelial growth factor	0.6	1.5	+ 2.5 ▲
bFGF	Basic fibroblast growth factor	22.6	54.8	+ 2.4 ▲
HB-EGF	Heparin-binding EGF-like growth factor	1.4	2.5	+ 1.8 ▲
TGF-β3	Transforming growth factor β3	2.8	4.0	+ 1.4 ▲
VEGF	Vascular endothelial growth factor	4.6	3.0	- 0.3 ▼
EGF R	Epidermal growth factor receptor	ND	ND	-

**Table 2 | Quantification of growth factors in IPF and normal lung matrix scaffolds.** Growth factor concentrations were measured by multiplex growth factor array. Green arrow (▲) indicates positive fold change (increase) from normal in concentration of growth factors. Red arrow (▼) indicates negative fold change (decrease) from normal in concentration of growth factors. ND: not detected.

309 matrix scaffolds. Normal lung matrix scaffolds appeared translucent, with visible bronchial and  
310 vascular conduits and saccular structures throughout the parenchyma (**Fig. 4A**). By contrast, IPF  
311 matrix scaffolds had pervasive dense fibroconnective structures, with abnormal disorganized  
312 architecture, honeycombing, and no apparent airways or vessels. Scanning electron microscopy  
313 revealed dramatic disruption of normal alveolar architecture in IPF scaffolds (**Fig. 4B**).  
314 Topography of collagen fibers in IPF scaffolds was visualized by inverted color micrographs of  
315 trichrome staining, which showed dense fibrous bundles in IPF scaffolds and stereotypical porous  
316 (alveolar-like) networks in normal lung scaffolds (**Fig. 4C**). Transmission electron microscopy  
317 showed dense fibrous bands (F) of extracellular matrix in IPF matrix scaffolds with minimal  
318 evidence of normal basement membrane, whereas normal lung matrix scaffolds had abundant  
319 airspaces (A), delicate basement membrane (arrow), and alveolar capillaries (C; **Fig. 4D**).  
320 Uniaxial mechanical testing of IPF and normal tissues and scaffolds indicated that IPF tissues  
321 and scaffolds were approximately 20× stiffer at 5% strain and approximately 5× stiffer at 20%  
322 strain compared to normal tissues and scaffolds (**Fig. 4E**). Importantly, mechanical testing also  
323 confirmed that the processing of native tissues to obtain matrix scaffolds did not alter the  
324 mechanical properties of matrix scaffolds from native tissues, as differences in elastic modulus  
325 between native tissues and matrix scaffolds were not significant (**Fig. 4F,G**).

326

327 **IPF matrix scaffolds support disease-like phenotype of lung fibroblasts.** Normal human lung  
328 fibroblasts were added to IPF and normal lung matrix scaffolds and cultured *in vitro* for 7 days.  
329 H&E staining showed that the phenotype of normal human lung fibroblasts varied between cells  
330 cultured in IPF and normal lung matrix scaffolds (**Fig. 5A**). Fibroblasts in IPF matrix scaffolds  
331 showed higher expression of alpha smooth muscle actin than fibroblasts in normal lung matrix  
332 scaffolds. Morphologic similarities between fibroblasts cultured in IPF scaffolds and IPF native  
333 tissue were observed (**Fig. 5B**). In contrast, immunostaining of FOXO3, a transcription factor  
334 whose downregulation is linked to fibrogenesis<sup>34</sup>, showed lower expression in human lung

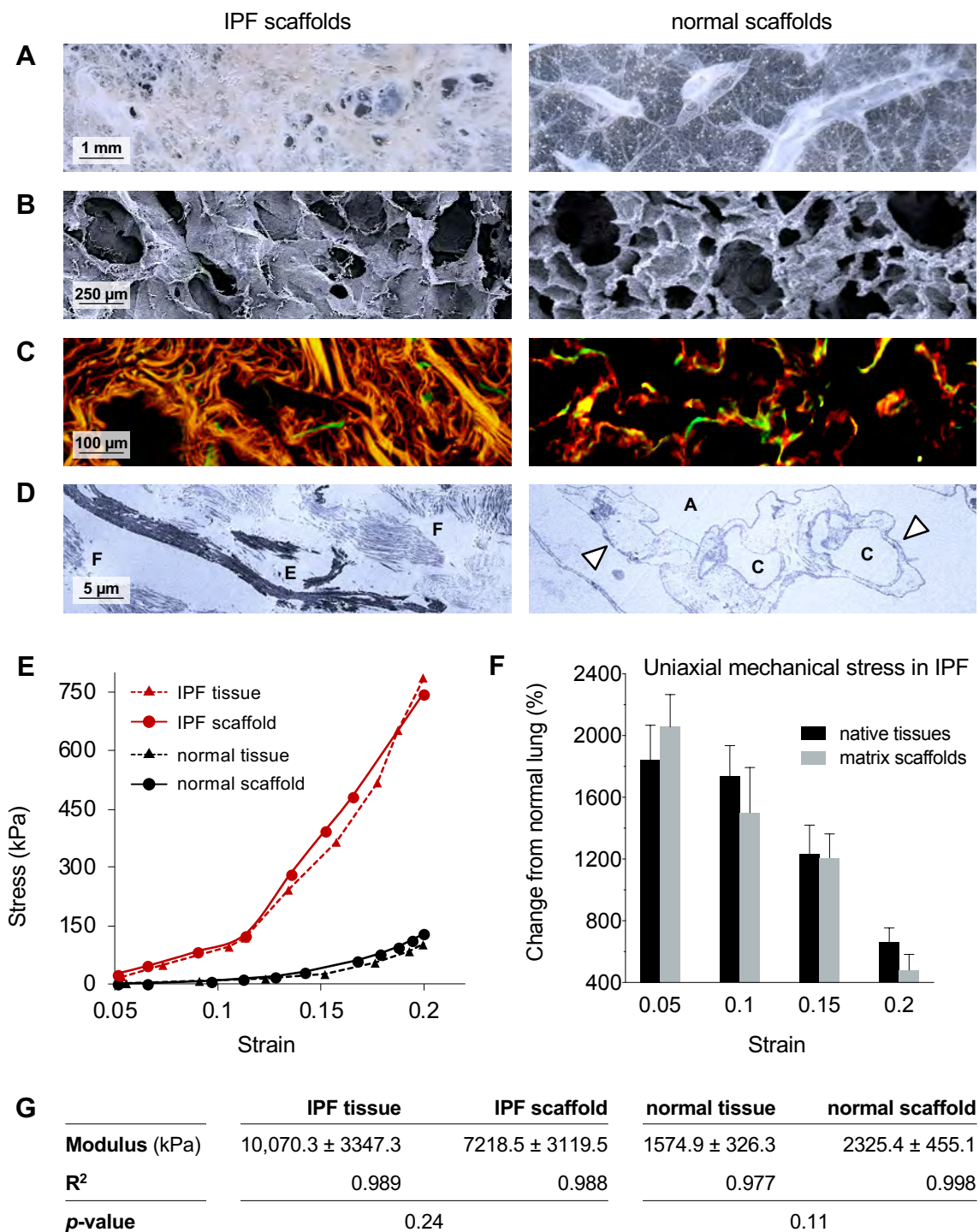


**Figure 4 | Structural, topographical, and mechanical characterizations of IPF lung scaffolds.** Representative images of IPF and normal lung scaffolds: (A) gross photograph, (B) scanning electron microscopy, (C) light microscopy (inverted color micrograph) of trichome staining demonstrating topography of ECM fibers in IPF scaffolds, (D) transmission electron microscopy. A: airspace, C: alveolar capillary, E: elastin bundle fragments, F: fibroconnective collagenous matrix, arrow: basement membrane. (E) Representative uniaxial stress-strain curves of IPF and normal lung tissues and matrix scaffolds. (F) Change in uniaxial mechanical stress from normal lung tissues and matrix scaffolds. (G) Tangent modulus values. Statistical analyses between tissues and scaffolds were performed using Student's *t*-test, with significance when  $p < 0.05$ . All values represent mean ± standard deviation.

335 fibroblasts cultured on IPF matrix scaffolds compared to fibroblasts cultured on normal lung matrix  
336 scaffolds (**Fig. 5C**). Consistent with alpha smooth muscle immunohistochemical staining, gene  
337 expression analysis showed significant upregulation of ACTA2 (alpha smooth muscle actin).  
338 Additional upregulated fibrosis-specific markers of fibroblast activation included COL1A1  
339 (collagen type I, subunit  $\alpha 1$ ), MMP2, PDGFC, PTEN, and PRRX1 (**Fig. 5D**). Activation of  
340 fibroblasts *in vitro* was also assessed by quantification of secreted basic fibroblast growth factor  
341 (bFGF) and transforming growth factor beta (TGF $\beta$ ), with normal human lung fibroblasts cultured  
342 on tissue culture plastic as a standard control. Interestingly, secretion of bFGF and TGF $\beta$  were  
343 both highest with fibroblasts cultured in IPF matrix scaffolds (**Fig. 5E,F**). Notably, secreted TGF $\beta$   
344 was significantly higher in IPF matrix scaffolds compared to normal lung matrix scaffolds,  
345 suggesting that substrate stiffness may have influenced secretion of TGF $\beta$ .

346

#### 347 **IPF matrix scaffolds provide a disease-specific environment for testing antifibrotic agents.**

348 Pulmonary fibroblasts in IPF matrix scaffolds showed a mean growth rate (linear fit: slope = 6.74,  
349  $R^2 = 0.98$ ) over 80% faster than fibroblasts in normal lung matrix scaffolds (linear fit: slope = 3.70,  
350  $R^2 = 0.93$ ; **Fig. 6A**, no drug), consistent with the fibroproliferative process characteristic of human  
351 IPF. To assess differences in phenotype between fibroblasts cultured on IPF matrix scaffolds and  
352 the conventional drug testing substrate tissue culture plastic, disease-associated gene expression  
353 and growth factor secretion were analyzed. Fibroblasts cultured in IPF matrix scaffolds expressed  
354 significantly higher COL1A1 and MMP2 than fibroblasts cultured on plastic (**Fig. 6B**), and  
355 secreted more profibrotic growth factors bFGF and TGF $\beta$  than fibroblasts cultured in normal lung  
356 matrix or on plastic (**Fig. 6C,D**), suggesting that the presence of disease-specific matrix resulted  
357 in more disease-associated fibroblast phenotype *in vitro* compared to fibroblasts on plastic. When  
358 exposed to antifibrotic agent PF3644022, a potent ATP-competitive MK2 inhibitor, pulmonary  
359 fibroblasts cultured in IPF matrix scaffolds demonstrated significant reduction in cell number  
360 compared to untreated fibroblasts over 6 days. PF3644022 also reduced expression of key IPF-



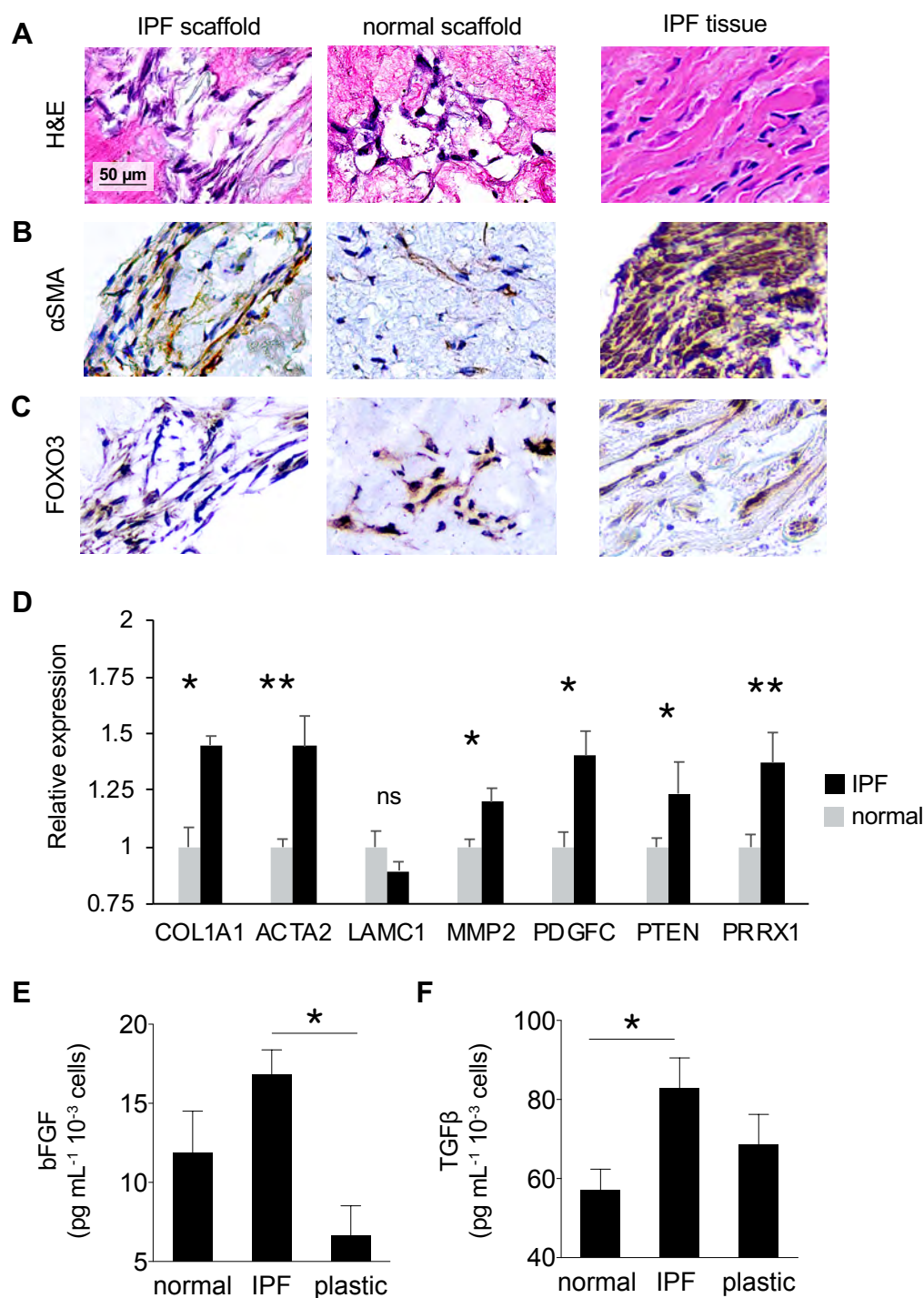


**Figure 5 | Phenotype of lung fibroblasts in IPF and normal lung scaffolds.** Representative micrographs of (A) H&E and immunohistochemical staining of (B) alpha smooth muscle actin (αSMA) and (C) Forkhead box O3 (FOXO3). (D) Gene expression of normal human lung fibroblasts cultured in IPF and normal lung scaffolds. \*  $p < 0.05$ , \*\*  $p < 0.01$ , ns: not significant. Quantification by ELISA of (E) basic fibroblast growth factor (bFGF, \*  $p < 0.05$ ) and (F) transforming growth factor beta (TGFβ, \*  $p < 0.05$ ) secreted by normal human lung fibroblast cultured in IPF and normal lung scaffolds and on tissue culture plastic. All values represent mean  $\pm$  standard deviation.

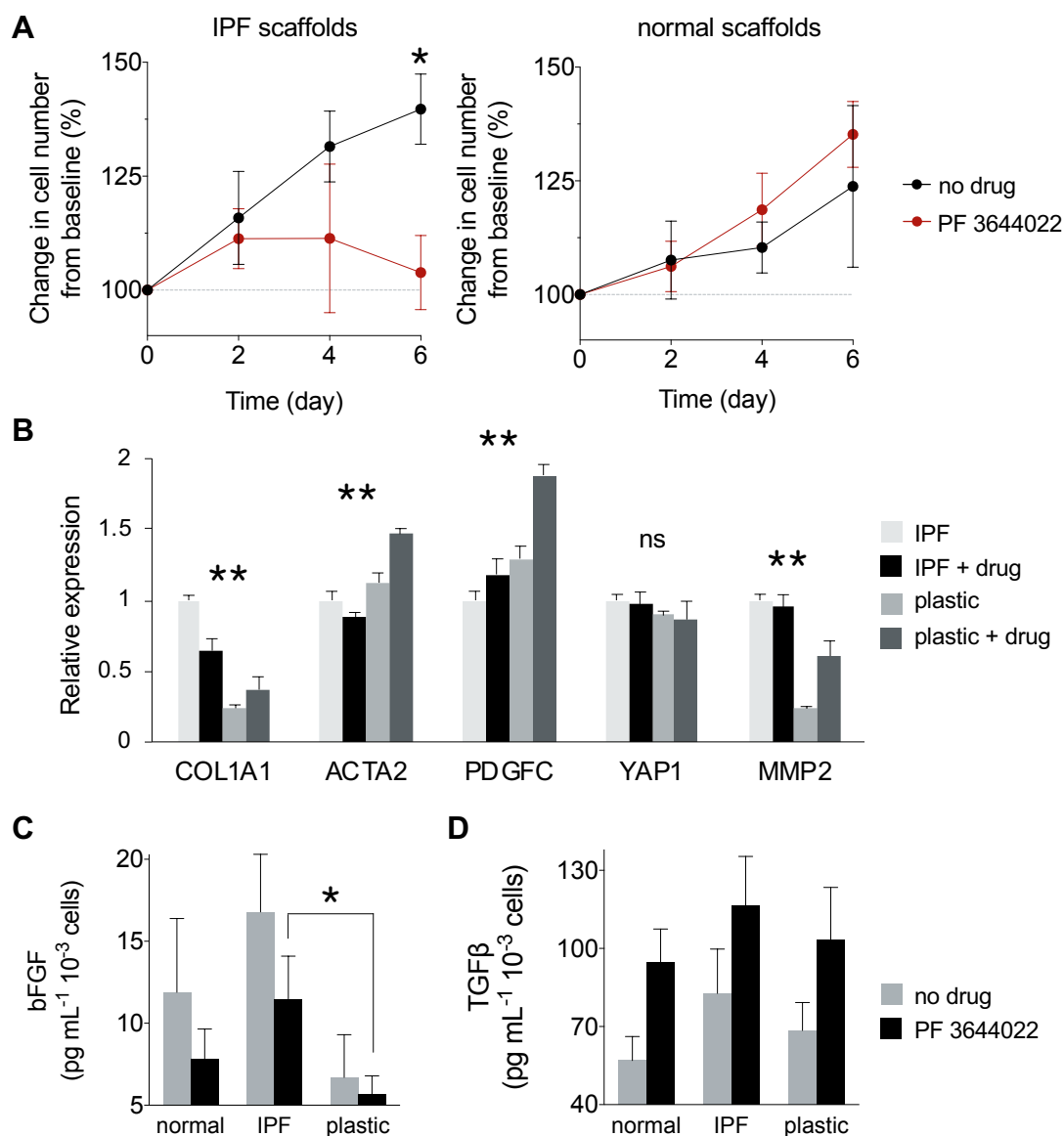


**Figure 6 | Demonstration of anti-fibrotic drug testing in IPF lung scaffolds.** (A) Growth curves of normal human lung fibroblasts over 6 days of treatment with PF 3644022. (B) Gene expression of normal human lung fibroblasts cultured on IPF scaffolds and tissue culture plastic. \*  $p < 0.05$ , \*\*  $p < 0.01$ . Quantification by ELISA of (C) basic fibroblast growth factor (bFGF,  $p = 0.0024$  by ANOVA) and (D) transforming growth factor beta (TGFβ,  $p = 0.0084$  by ANOVA) secreted by normal lung fibroblast cultured in IPF and normal lung scaffolds and on tissue culture plastic. All values represent mean  $\pm$  standard deviation.



361 associated genes COL1A1 and ACTA2 by fibroblasts in IPF matrix scaffolds (**Fig. 6B**) – an  
362 expected result not observed in fibroblasts cultured on plastic. Similarly, PF3644022 reduced  
363 secretion of bFGF by fibroblasts cultured in IPF matrix scaffolds (**Fig. 6C**). Interestingly, secretion  
364 of TGF $\beta$  by fibroblasts exposed to PF3644022 trended upward across all substrates (**Fig. 6D**).  
365 Altogether, these results confirm the activation and diseased phenotype of pulmonary fibroblasts  
366 cultured in IPF matrix, and demonstrate the feasibility of testing antifibrotic agents in an *in-vitro*  
367 substrate environment with IPF disease-specific features not otherwise present in tissue culture  
368 plastic or other conventional drug screening platforms.

369

## 370 **DISCUSSION**

371

372 Using a physiomimetic approach, we developed an IPF disease-specific 3D cell culture substrate  
373 comprised of fibrotic human lung extracellular matrix. Through biomolecular and physico-  
374 mechanical characterizations, we show that this disease-specific substrate has numerous  
375 physical and compositional features of the human IPF diseased extracellular matrix environment.  
376 We also demonstrate the applicability of this substrate for pharmaceutical drug testing. As the  
377 critical need for effective IPF drugs persists, human IPF disease-specific cell culture substrates  
378 could enable more predictive disease models and drug screening platforms, and accelerate  
379 development of new drugs for the treatment of IPF.

380

381 Human IPF is a chronic, aging-related disease of unknown etiology typically diagnosed at an  
382 advanced stage, and is therefore challenging to model. Both animal<sup>10,13</sup> and *in-vitro* models<sup>18,19,35-</sup>  
383 <sup>37</sup> have been used to gain insights into the cellular and molecular mechanisms of IPF. Although  
384 animal models of IPF have been developed in mice, rats, hamsters, guinea pigs, rabbits, cats,  
385 dogs, sheep, donkeys, horses, and non-human primates,<sup>11,38-40</sup> no animal model fully  
386 recapitulates the pathophysiology of human IPF – specifically, the histologic pattern of usual

387 interstitial pneumonia and progressive fibrotic disease.<sup>13</sup> Furthermore, while animal models may  
388 inform various aspects of fibrotic lung disease, significant anatomical, biological, and  
389 immunological differences from humans reduce pathophysiological relevance to human IPF.  
390 Notably, the American Thoracic Society has emphasized the importance of developing  
391 'humanized' models of IPF to increase relevance of animal models of IPF to the human disease.<sup>41</sup>

392

393 Because animal models of IPF are inherently limited, *in-vitro* models are an indispensable tool in  
394 basic and translational studies of human IPF. Previous studies have implicated multiple cellular  
395 processes in pulmonary fibrosis including epithelial cell apoptosis<sup>42</sup>, epithelial–mesenchymal  
396 transition<sup>43</sup>, and differentiation of fibroblasts to myofibroblasts<sup>44</sup> that result in significant  
397 remodeling and deposition of fibrotic ECM. Conventional two-dimensional (2D) models of IPF  
398 typically utilize monolayers of pulmonary myofibroblasts, the primary effector cells of IPF<sup>45</sup>, on  
399 tissue culture plastic, enabling mechanistic studies in controlled experimental settings. However,  
400 cells cultured in 2D models experience artificial, non-physiological conditions that categorically  
401 lack the appropriate three-dimensional (3D) spatial gradients – chemical, mechanical,  
402 topographical – in which all lung cells naturally reside within the body. Constrained to one spatial  
403 plane, cells in 2D models are immobilized, experience limited cell–cell interactions, and display  
404 inhibited cytokinesis and chemotaxis, artificial flattened morphology, unnatural apical-basal  
405 polarization, and abnormal integrin and cell-surface receptor expression and distribution.<sup>46-48</sup>  
406 Furthermore, tissue culture plastic has non-physiological topography and stiffness (> 1,000  
407 kPa)<sup>49</sup>, which has been shown to drive atypical cytoskeletal rearrangements<sup>50</sup>, perturb  
408 homeostatic gene expression<sup>51</sup>, and induce epigenetic modifications of fibroblasts<sup>52</sup>.

409  
410 Pulmonary fibroblasts cultured in 3D models, however, adhere to substrates at multiple focal  
411 adhesion points<sup>53</sup>, and experience more *in vivo*-like stress–strain<sup>47</sup> and soluble<sup>54</sup> gradients. Lung  
412 fibroblasts cultured in hydrogels of collagen type I, a structural ECM component upregulated in

413 IPF, previously displayed contraction of collagen hydrogels, whose resistance to cell-generated  
414 forces was proportional to expression of  $\alpha$ SMA by fibroblasts.<sup>55</sup> Notably, collagen type I hydrogels  
415 are comprised of a single structural ECM component, and thus lack the complex signaling and  
416 regulation of the multi-component ECM in the fibrotic disease environment. As paracrine, cell–  
417 cell, and cell–matrix interactions are known to drive progression of fibrotic lung disease,<sup>56</sup> disease-  
418 specific 3D cell culture substrates are critical for improving *in-vitro* models of IPF, and should  
419 ideally recapitulate the structure, mechanics, and biochemical composition of diseased human  
420 lung tissue.

421  
422 In this study, biochemical and mass spectrometry analyses confirmed that IPF matrix scaffolds  
423 had: (i) increased collagens and decreased elastin consistent with increased stiffness and  
424 decreased compliance, (ii) increased proteoglycans, whose covalently bound glycosaminoglycan  
425 side chains chondroitin sulfate, dermatan sulfate, heparan sulfate, and hyaluronic acid have been  
426 shown to be structurally altered and increased in IPF lungs<sup>57</sup>, and (iii) abnormal profile of  
427 glycoproteins. Proteoglycans influence viscoelastic properties, cell differentiation, and tissue  
428 morphogenesis, and in particular heparan sulfate coordinates ligand–receptor binding of FGF,  
429 PDGF, TGF $\beta$ , and VEGF<sup>58</sup> – growth factors involved in pathologic tissue remodeling and detected  
430 in IPF matrix scaffolds. Biglycan, a small leucine-rich proteoglycan (SLRP) known to be altered in  
431 fibrosis and correlated with lung mechanics through influence on ECM assembly<sup>59</sup>, was increased  
432 over 600% in IPF matrix scaffolds. The perturbed profile of glycoproteins in IPF matrix scaffolds  
433 included: increased fibrillin 2, a collagenase-resistant glycoprotein that is associated with the 10-  
434 nm microfibrils of the basal lamina and regulates the bioavailability of TGF $\beta$  through latent  
435 transforming growth factor  $\beta$  binding proteins (LTBP)<sup>60</sup>, and increased periostin, a matricellular  
436 glycoprotein that promotes fibroblast proliferation, localization of fibrogenic growth factors,  
437 collagen type I production, and collagen crosslinking<sup>61</sup>. Notably, the loss of basement membrane  
438 components including collagen type IV<sup>29</sup>, laminin, and nidogen in IPF tissues and matrix scaffolds

439 suggests that the use of basement membrane extracts such as Matrigel in models of IPF has  
440 minimal pathophysiologic relevance.

441  
442 The stiffness of fibrotic lung tissue ( $60 \pm 40$  kPa) is significantly higher than the stiffness of normal  
443 lung tissue ( $7 \pm 6$  kPa)<sup>35,49</sup>, which has critical implications for the stiffness of cell culture substrates  
444 in models of IPF, especially for *in-vitro* culture of pulmonary fibroblasts, which exhibit complex  
445 mechanotransduction<sup>20,62</sup> and have ‘mechanical memory’<sup>63</sup>. In this study, fibrotic human lung  
446 ECM scaffolds recapitulated the mechanical differences between normal and fibrotic lung tissues  
447 (**Fig. 4**), and supported increased secretion of bFGF and TGF $\beta$  by normal human lung fibroblasts  
448 (**Fig. 5E,F**), suggesting that the IPF matrix scaffolds have disease-specific mechanics and  
449 regulatory signals relevant to human IPF. Notably, pulmonary fibroblasts cultured in fibrotic lung  
450 ECM previously confirmed the regulatory role of ECM in the activation of myofibroblasts *in vitro*<sup>36</sup>,  
451 and demonstrated significant effects of substrate stiffness on fibroblast activation and  
452 differentiation into myofibroblasts. Myofibroblast differentiation has also been shown to be driven  
453 by increased ECM stiffness through mechanisms independent of TGF $\beta$ <sup>20</sup>. Interestingly, previous  
454 studies wherein normal and IPF fibroblasts were cultured across ECM from normal and IPF lungs  
455 revealed that IPF ECM had a greater influence on fibroblast gene expression than cell origin<sup>64</sup>,  
456 further indicating the central role of ECM in regulating disease-associated gene expression.  
457 Altogether, these results highlight the critical importance of providing disease-specific signals from  
458 the ECM environment in models of fibrotic lung disease.

459  
460 In spite of decades of basic and translational research, the persisting struggle to successfully  
461 translate promising preclinical drug candidates to drugs approved to treat IPF highlights the  
462 limited effectiveness of disease models used in IPF drug discovery, which is likely attributable to  
463 the failure of IPF models to recapitulate key pathophysiological features of the human disease.  
464 Early-stage drug discovery assays are typically conducted on tissue culture plastic (e.g.,

465 polystyrene) with or without collagen type I coating, and supplemental TGF $\beta$  (e.g., 1 – 5 ng mL<sup>-1</sup>)  
466 to activate primary or immortalized human lung fibroblasts – an entrenched *in-vitro* system that  
467 has minimal pathophysiological relevance to the human IPF disease setting. With significant  
468 financial costs and scientific, medical, and regulatory challenges associated with conducting  
469 clinical trials in patients with IPF, preclinical assessments of antifibrotic compounds must be  
470 sufficiently robust to inform go/no go decision making and yield reliably predictive data in order to  
471 maximize the likelihood of advancing promising drug candidates to clinical trials.

472

473 In this study, we demonstrated the use of IPF disease-specific ECM in a 3D cell-based assay of  
474 antifibrotic agent PF3644022 (an MK2 inhibitor in IPF model)<sup>65</sup>. As expected, fibroblasts cultured  
475 on fibrotic lung ECM scaffolds and treated with PF3644022 exhibited greater sensitivity and drug  
476 response, significantly different gene expression, and downregulation of genes associated with  
477 ECM production compared to cells cultured on tissue culture plastic. We envision that disease-  
478 specific ECM may be applicable across multiple stages of the drug discovery pipeline, from target  
479 selection and hit identification through lead identification and optimization. The use of disease-  
480 specific ECM substrates is consistent with the set of principles<sup>66</sup> defined for 'disease-relevant  
481 assays' that specifically recommend ensuring: (i) substrate tension and mechanical forces are  
482 appropriate, and (ii) extracellular matrix composition is relevant, with appropriate tissue  
483 architecture, cell differentiation and function to enhance clinical translation of the *in-vitro* assay.  
484 Ultimately, implementation of disease-specific ECM components or substrates into preclinical  
485 human disease models and cell-based screening assays could increase clinical relevance and  
486 success rates.

487

488 There are several limitations to the present study: (1) This study investigated a small number of  
489 human lungs ( $n = 6$  total,  $n = 3$  per group). Although this study was conducted with the minimum  
490 number of human lungs required to achieve statistical significance between groups, investigation

491 of larger numbers of IPF lungs would offer opportunities for deeper statistical analyses and  
492 potential correlations between matrix characteristics and disease phenotypes. (2) As IPF lung  
493 specimens were procured from explanted tissues following lung transplantation, this study only  
494 investigated fibrotic lung matrix from end-stage disease. While diagnosis of IPF remains a  
495 significant clinical challenge, procurement of fibrotic human lung ECM at earlier stages of fibrotic  
496 disease may not be feasible. (3) Human donor tissues present intrinsic biological variability that  
497 could confound experimental results. To minimize variability between donors, acceptance criteria  
498 for lungs were tightly defined and strictly implemented. Furthermore, as IPF is a disease with  
499 demonstrable spatiotemporal heterogeneity, extensive histopathologic review was conducted by  
500 a lung transplant pathologist to ensure only tissues and scaffolds with fibrosis scores  $\geq 2$  were  
501 utilized. (4) Only one antifibrotic drug was evaluated in this study. Future studies will investigate  
502 additional compounds to provide further evidence of the utility and benefits of IPF disease-specific  
503 ECM substrates.

504  
505 The IPF matrix scaffolds developed in this study may be useful for cell-based assays, but may  
506 have limited applicability to high throughput drug screening systems, which typically utilize rapid  
507 optical readouts in 96- and 384-well plate formats. Therefore, an alternative format of fibrotic lung  
508 matrix, e.g., hydrogel, may be more suitable for high throughput applications. Future studies will  
509 explore the development of additional IPF disease-specific ECM formats to address broader  
510 research and development applications such as 'IPF-on-chip'. As IPF disease progression is  
511 driven by a combination of lung and immune cell–cell and cell–matrix interactions, future studies  
512 will also investigate co-cultures with pulmonary macrophages, epithelial and smooth muscle cells,  
513 and the effects of IPF-associated growth factors on lung cells *in vitro*. Altogether, an *in-vitro* model  
514 with a disease-specific substrate of human IPF disease environment can help elucidate  
515 underlying idiopathologies of IPF, enable development of effective IPF therapeutics, and may

516 serve as a template approach for the development of fibrosis-specific cell culture substrates in  
517 other human organs and tissues susceptible to fibrotic disease.

518

## 519 **CONCLUSIONS**

520 We developed a pulmonary fibrosis-specific cell culture substrate comprised of intact fibrotic lung  
521 extracellular matrix that recapitulated *in vitro* key features of the human IPF disease environment  
522 and supported the disease-associated phenotype of human lung fibroblasts. We also  
523 demonstrated feasibility of testing antifibrotic agents using this substrate, which may be applicable  
524 in cell-based assays in early-stage drug discovery.

525

## 526 **ACKNOWLEDGEMENTS**

527 The authors would like to thank M. Bacchetta and G. Vunjak–Novakovic for discussions of the  
528 experimental design and results; M. Bacchetta and Y. Tipograf for coordinating receipt of human  
529 lung tissues; Albert Einstein College of Medicine Analytical Imaging Facility for slide scanning; C.  
530 Marboe for conducting blinded pathologic assessments; and Weill Cornell Microscopy and Image  
531 Analysis Core Facility staff, including L. Cohen-Gould and J. P. Jimenez for transmission electron  
532 microscopy imaging services. The authors gratefully acknowledge funding support  
533 (1R43HL144341) from the National Institutes of Health.

534

## 535 **AUTHOR CONTRIBUTIONS**

536 I.G., E.A., and J.D.O. designed the study. I.G., E.A., J. X., N. K., A. N., and E.G. performed  
537 experiments. I.G., E.A., and J.D.O. co-analyzed data, co-wrote the manuscript.

538 **REFERENCES**

539

540 1 Lederer, D. J. & Martinez, F. J. Idiopathic Pulmonary Fibrosis. *N Engl J Med* **378**, 1811-  
541 1823, doi:10.1056/NEJMra1705751 (2018).

542 2 Coward, W. R., Saini, G. & Jenkins, G. The pathogenesis of idiopathic pulmonary fibrosis.  
543 *Thor Adv Respir Dis* **4**, 367-388, doi:10.1177/1753465810379801 (2010).

544 3 Noble, P. W., Barkauskas, C. E. & Jiang, D. Pulmonary fibrosis: patterns and perpetrators.  
545 *J Clin Invest* **122**, 2756-2762, doi:10.1172/JCI60323 (2012).

546 4 Sauleda, J., Nunez, B., Sala, E. & Soriano, J. B. Idiopathic Pulmonary Fibrosis:  
547 Epidemiology, Natural History, Phenotypes. *Med Sci (Basel)* **6**,  
548 doi:10.3390/medsci6040110 (2018).

549 5 Ley, B. & Collard, H. R. Epidemiology of idiopathic pulmonary fibrosis. *Clin Epidemiol* **5**,  
550 483-492, doi:10.2147/CLEP.S54815 (2013).

551 6 Hutchinson, J., Fogarty, A., Hubbard, R. & McKeever, T. Global incidence and mortality of  
552 idiopathic pulmonary fibrosis: a systematic review. *Eur Respir J* **46**, 795-806,  
553 doi:10.1183/09031936.00185114 (2015).

554 7 Vancheri, C., Failla, M., Crimi, N. & Raghu, G. Idiopathic pulmonary fibrosis: a disease with  
555 similarities and links to cancer biology. *Eur Respir J* **35**, 496-504,  
556 doi:10.1183/09031936.00077309 (2010).

557 8 Ryu, J. H. *et al.* Idiopathic pulmonary fibrosis: evolving concepts. *Mayo Clin Proc* **89**, 1130-  
558 1142, doi:10.1016/j.mayocp.2014.03.016 (2014).

559 9 Plantier, L. *et al.* Physiology of the lung in idiopathic pulmonary fibrosis. *Eur Respir Rev* **27**,  
560 doi:10.1183/16000617.0062-2017 (2018).

561 10 Moore, B. B. & Hogaboam, C. M. Murine models of pulmonary fibrosis. *Am J Physiol Lung*  
562 *Cell Mol Physiol* **294**, L152-160, doi:10.1152/ajplung.00313.2007 (2008).



- 563 11 Mouratis, M. A. & Aidinis, V. Modeling pulmonary fibrosis with bleomycin. *Curr Opin Pulm*  
564 *Med* **17**, 355-361, doi:10.1097/MCP.0b013e328349ac2b (2011).
- 565 12 Antje Moeller, J. C. R.-L., Lingqiao Wang, Jack Gauldie, Martin Kolb. Models of pulmonary  
566 fibrosis. *Drug Discovery Today Disease Models* **3**, 243-249 (2006).
- 567 13 B, B. M. *et al.* Animal models of fibrotic lung disease. *Am J Respir Cell Mol Biol* **49**, 167-  
568 179, doi:10.1165/rcmb.2013-0094TR (2013).
- 569 14 Nichols, J. E., Niles, J. A., Vega, S. P. & Cortiella, J. Novel in vitro respiratory models to  
570 study lung development, physiology, pathology and toxicology. *Stem Cell Res Ther* **4**  
571 **Suppl 1**, S7, doi:10.1186/scri368 (2013).
- 572 15 Zhou, Y. *et al.* Extracellular matrix in lung development, homeostasis and disease. *Matrix*  
573 *Biol* **73**, 77-104, doi:10.1016/j.matbio.2018.03.005 (2018).
- 574 16 Shimbori, C., Gauldie, J. & Kolb, M. Extracellular matrix microenvironment contributes  
575 actively to pulmonary fibrosis. *Curr Opin Pulm Med* **19**, 446-452,  
576 doi:10.1097/MCP.0b013e328363f4de (2013).
- 577 17 Kristensen, J. H. *et al.* The role of extracellular matrix quality in pulmonary fibrosis.  
578 *Respiration* **88**, 487-499, doi:10.1159/000368163 (2014).
- 579 18 Hetzel, M., Bachem, M., Anders, D., Trischler, G. & Faehling, M. Different effects of growth  
580 factors on proliferation and matrix production of normal and fibrotic human lung fibroblasts.  
581 *Lung* **183**, 225-237, doi:10.1007/s00408-004-2534-z (2005).
- 582 19 Correll, K. A. *et al.* TGF beta inhibits HGF, FGF7, and FGF10 expression in normal and IPF  
583 lung fibroblasts. *Physiol Rep* **6**, e13794, doi:10.14814/phy2.13794 (2018).
- 584 20 Huang, X. *et al.* Matrix stiffness-induced myofibroblast differentiation is mediated by  
585 intrinsic mechanotransduction. *Am J Respir Cell Mol Biol* **47**, 340-348,  
586 doi:10.1165/rcmb.2012-0050OC (2012).

- 587 21 Wight, T. N. & Potter-Perigo, S. The extracellular matrix: an active or passive player in  
588 fibrosis? *Am J Physiol Gastrointest Liver Physiol* **301**, G950-955,  
589 doi:10.1152/ajpgi.00132.2011 (2011).
- 590 22 Lehtonen, S. T. *et al.* Pirfenidone and nintedanib modulate properties of fibroblasts and  
591 myofibroblasts in idiopathic pulmonary fibrosis. *Respir Res* **17**, 14, doi:10.1186/s12931-  
592 016-0328-5 (2016).
- 593 23 O'Neill, J. D. *et al.* Decellularization of human and porcine lung tissues for pulmonary tissue  
594 engineering. *Ann Thorac Surg* **96**, 1046-1055; discussion 1055-1046,  
595 doi:10.1016/j.athoracsur.2013.04.022 (2013).
- 596 24 Wagner, D. E. *et al.* Three-dimensional scaffolds of acellular human and porcine lungs for  
597 high throughput studies of lung disease and regeneration. *Biomaterials* **35**, 2664-2679,  
598 doi:10.1016/j.biomaterials.2013.11.078 (2014).
- 599 25 Balestrini, J. L. *et al.* Comparative biology of decellularized lung matrix: Implications of  
600 species mismatch in regenerative medicine. *Biomaterials* **102**, 220-230,  
601 doi:10.1016/j.biomaterials.2016.06.025 (2016).
- 602 26 Gilpin, S. E. & Wagner, D. E. Acellular human lung scaffolds to model lung disease and  
603 tissue regeneration. *Eur Respir Rev* **27**, doi:10.1183/16000617.0021-2018 (2018).
- 604 27 Ashcroft, T., Simpson, J. M. & Timbrell, V. Simple method of estimating severity of  
605 pulmonary fibrosis on a numerical scale. *J Clin Pathol* **41**, 467-470,  
606 doi:10.1136/jcp.41.4.467 (1988).
- 607 28 Lu, J., Auduong, L., White, E. S. & Yue, X. Up-regulation of heparan sulfate 6-O-sulfation in  
608 idiopathic pulmonary fibrosis. *Am J Respir Cell Mol Biol* **50**, 106-114,  
609 doi:10.1165/rcmb.2013-0204OC (2014).
- 610 29 Sand, J. M. *et al.* MMP mediated degradation of type IV collagen alpha 1 and alpha 3  
611 chains reflects basement membrane remodeling in experimental and clinical fibrosis--

- 612 validation of two novel biomarker assays. *PLoS One* **8**, e84934,  
613 doi:10.1371/journal.pone.0084934 (2013).
- 614 30 S. Ohshimo, K. H., F. Bonella, C. Yamaoka, Y. Horimasu, H. Iwamoto, N. Ishikawa, K.  
615 Fujitaka, H. Murai, H. Hamada, N. Hattori, N. Hirohashi, K. Tanigawa, J. Guzman, U.  
616 Costabel, N. Kohno. Growth Differentiation Factor-15 (gdf-15) As Prognostic Factor For  
617 Idiopathic Pulmonary Fibrosis. *Am J Respir Crit Care Med* **191** (2015).
- 618 31 Ruan, W. & Ying, K. Abnormal expression of IGF-binding proteins, an initiating event in  
619 idiopathic pulmonary fibrosis? *Pathol Res Pract* **206**, 537-543,  
620 doi:10.1016/j.prp.2010.03.010 (2010).
- 621 32 Pilewski, J. M., Liu, L., Henry, A. C., Knauer, A. V. & Feghali-Bostwick, C. A. Insulin-like  
622 growth factor binding proteins 3 and 5 are overexpressed in idiopathic pulmonary fibrosis  
623 and contribute to extracellular matrix deposition. *Am J Pathol* **166**, 399-407,  
624 doi:10.1016/S0002-9440(10)62263-8 (2005).
- 625 33 Avcuoglu, S. *et al.* Neurotrophic tyrosine kinase receptor B/neurotrophin 4 signaling axis is  
626 perturbed in clinical and experimental pulmonary fibrosis. *Am J Respir Cell Mol Biol* **45**,  
627 768-780, doi:10.1165/rcmb.2010-0195OC (2011).
- 628 34 Al-Tamari, H. M. *et al.* FoxO3 an important player in fibrogenesis and therapeutic target for  
629 idiopathic pulmonary fibrosis. *EMBO Mol Med* **10**, 276-293,  
630 doi:10.15252/emmm.201606261 (2018).
- 631 35 Hinz, B. Mechanical aspects of lung fibrosis: a spotlight on the myofibroblast. *Proc Am*  
632 *Thorac Soc* **9**, 137-147, doi:10.1513/pats.201202-017AW (2012).
- 633 36 Booth, A. J. *et al.* Acellular normal and fibrotic human lung matrices as a culture system for  
634 in vitro investigation. *Am J Respir Crit Care Med* **186**, 866-876, doi:10.1164/rccm.201204-  
635 0754OC (2012).

- 636 37 Thannickal, V. J. *et al.* Matrix biology of idiopathic pulmonary fibrosis: a workshop report of  
637 the national heart, lung, and blood institute. *Am J Pathol* **184**, 1643-1651,  
638 doi:10.1016/j.ajpath.2014.02.003 (2014).
- 639 38 Tashiro, J. *et al.* Exploring Animal Models That Resemble Idiopathic Pulmonary Fibrosis.  
640 *Front Med (Lausanne)* **4**, 118, doi:10.3389/fmed.2017.00118 (2017).
- 641 39 Paul F. Mercer, K. A.-B., Ian M. Adcock, Richard G. Knowles. Translational models of lung  
642 disease. *Clinical Science* **128** 235-256, doi:10.1042/CS20140373 (2015).
- 643 40 Organ, L. *et al.* A novel segmental challenge model for bleomycin-induced pulmonary  
644 fibrosis in sheep. *Exp Lung Res* **41**, 115-134, doi:10.3109/01902148.2014.985806 (2015).
- 645 41 R. Gisli Jenkins, B. B. M., Rachel C. Chambers, Oliver Eickelberg, Melanie Konigshoff,  
646 Martin Kolb, Geoffrey J. Laurent, Carmel B. Nanthakumar, Mitchell A. Olman, Annie Pardo,  
647 Moises Selman, Dean Sheppard, Patricia J. Sime, Andrew M. Tager, Amanda L. Tatler,  
648 Victor J. Thannickal, and Eric S. White; on behalf of the ATS Assembly on Respiratory Cell  
649 and Molecular Biology. An Official American Thoracic Society Workshop Report: Use of  
650 Animal Models for the Preclinical Assessment of Potential Therapies for Pulmonary  
651 Fibrosis. *Am J Respir Cell Mol Biol* **56**, 667-679, doi:10.1165/rcmb.2017-0096ST (2017).
- 652 42 Lepparanta, O. *et al.* Regulation of TGF-beta storage and activation in the human idiopathic  
653 pulmonary fibrosis lung. *Cell Tissue Res* **348**, 491-503, doi:10.1007/s00441-012-1385-9  
654 (2012).
- 655 43 Kim, K. K. *et al.* Alveolar epithelial cell mesenchymal transition develops in vivo during  
656 pulmonary fibrosis and is regulated by the extracellular matrix. *Proc Natl Acad Sci U S A*  
657 **103**, 13180-13185, doi:10.1073/pnas.0605669103 (2006).
- 658 44 Kis, K., Liu, X. & Hagood, J. S. Myofibroblast differentiation and survival in fibrotic disease.  
659 *Expert Rev Mol Med* **13**, e27, doi:10.1017/S1462399411001967 (2011).
- 660 45 Todd, N. W., Luzina, I. G. & Atamas, S. P. Molecular and cellular mechanisms of  
661 pulmonary fibrosis. *Fibrogenesis Tissue Repair* **5**, 11, doi:10.1186/1755-1536-5-11 (2012).

- 662 46 Sundarakrishnan, A., Chen, Y., Black, L. D., Aldridge, B. B. & Kaplan, D. L. Engineered cell  
663 and tissue models of pulmonary fibrosis. *Adv Drug Deliv Rev* **129**, 78-94,  
664 doi:10.1016/j.addr.2017.12.013 (2018).
- 665 47 Baker, B. M. & Chen, C. S. Deconstructing the third dimension: how 3D culture  
666 microenvironments alter cellular cues. *J Cell Sci* **125**, 3015-3024, doi:10.1242/jcs.079509  
667 (2012).
- 668 48 Griffith, L. G. & Swartz, M. A. Capturing complex 3D tissue physiology in vitro. *Nat Rev Mol*  
669 *Cell Biol* **7**, 211-224, doi:10.1038/nrm1858 (2006).
- 670 49 Skardal, A., Mack, D., Atala, A. & Soker, S. Substrate elasticity controls cell proliferation,  
671 surface marker expression and motile phenotype in amniotic fluid-derived stem cells. *J*  
672 *Mech Behav Biomed Mater* **17**, 307-316, doi:10.1016/j.jmbbm.2012.10.001 (2013).
- 673 50 Doyle, A. D. & Yamada, K. M. Mechanosensing via cell-matrix adhesions in 3D  
674 microenvironments. *Exp Cell Res* **343**, 60-66, doi:10.1016/j.yexcr.2015.10.033 (2016).
- 675 51 Raab, M., Shin, J. W. & Discher, D. E. Matrix elasticity in vitro controls muscle stem cell  
676 fate in vivo. *Stem Cell Res Ther* **1**, 38, doi:10.1186/scrt38 (2010).
- 677 52 Nestor, C. E. *et al.* Rapid reprogramming of epigenetic and transcriptional profiles in  
678 mammalian culture systems. *Genome Biol* **16**, 11, doi:10.1186/s13059-014-0576-y (2015).
- 679 53 Lou, J., Stowers, R., Nam, S., Xia, Y. & Chaudhuri, O. Stress relaxing hyaluronic acid-  
680 collagen hydrogels promote cell spreading, fiber remodeling, and focal adhesion formation  
681 in 3D cell culture. *Biomaterials* **154**, 213-222, doi:10.1016/j.biomaterials.2017.11.004  
682 (2018).
- 683 54 Klingberg, F. *et al.* Prestress in the extracellular matrix sensitizes latent TGF-beta1 for  
684 activation. *J Cell Biol* **207**, 283-297, doi:10.1083/jcb.201402006 (2014).
- 685 55 Arora, P. D., Narani, N. & McCulloch, C. A. The compliance of collagen gels regulates  
686 transforming growth factor-beta induction of alpha-smooth muscle actin in fibroblasts. *Am J*  
687 *Pathol* **154**, 871-882, doi:10.1016/s0002-9440(10)65334-5 (1999).

- 688 56 Barkauskas, C. E. & Noble, P. W. Cellular mechanisms of tissue fibrosis. 7. New insights  
689 into the cellular mechanisms of pulmonary fibrosis. *Am J Physiol Cell Physiol* **306**, C987-  
690 996, doi:10.1152/ajpcell.00321.2013 (2014).
- 691 57 Westergren-Thorsson, G. *et al.* Increased deposition of glycosaminoglycans and altered  
692 structure of heparan sulfate in idiopathic pulmonary fibrosis. *Int J Biochem Cell Biol* **83**, 27-  
693 38, doi:10.1016/j.biocel.2016.12.005 (2017).
- 694 58 Forsten-Williams, K., Chu, C. L., Fannon, M., Buczek-Thomas, J. A. & Nugent, M. A.  
695 Control of growth factor networks by heparan sulfate proteoglycans. *Ann Biomed Eng* **36**,  
696 2134-2148, doi:10.1007/s10439-008-9575-z (2008).
- 697 59 Faffe, D. S. & Zin, W. A. Lung parenchymal mechanics in health and disease. *Physiol Rev*  
698 **89**, 759-775, doi:10.1152/physrev.00019.2007 (2009).
- 699 60 Davis, M. R. & Summers, K. M. Structure and function of the mammalian fibrillin gene  
700 family: implications for human connective tissue diseases. *Mol Genet Metab* **107**, 635-647,  
701 doi:10.1016/j.ymgme.2012.07.023 (2012).
- 702 61 O'Dwyer, D. N. & Moore, B. B. The role of periostin in lung fibrosis and airway remodeling.  
703 *Cell Mol Life Sci* **74**, 4305-4314, doi:10.1007/s00018-017-2649-z (2017).
- 704 62 Branco da Cunha, C. *et al.* Influence of the stiffness of three-dimensional alginate/collagen-  
705 I interpenetrating networks on fibroblast biology. *Biomaterials* **35**, 8927-8936,  
706 doi:10.1016/j.biomaterials.2014.06.047 (2014).
- 707 63 Balestrini, J. L., Chaudhry, S., Sarrazy, V., Koehler, A. & Hinz, B. The mechanical memory  
708 of lung myofibroblasts. *Integrative Biology* **4**, 410-421, doi:10.1039/c2ib00149g (2012).
- 709 64 Parker, M. W. *et al.* Fibrotic extracellular matrix activates a profibrotic positive feedback  
710 loop. *J Clin Invest* **124**, 1622-1635, doi:10.1172/JCI71386 (2014).
- 711 65 Mourey, R. J. *et al.* A benzothiophene inhibitor of mitogen-activated protein kinase-  
712 activated protein kinase 2 inhibits tumor necrosis factor alpha production and has oral anti-

713 inflammatory efficacy in acute and chronic models of inflammation. *J Pharmacol Exp Ther*  
714 **333**, 797-807, doi:10.1124/jpet.110.166173 (2010).  
715 66 Horvath, P. *et al.* Screening out irrelevant cell-based models of disease. *Nat Rev Drug*  
716 *Discov* **15**, 751-769, doi:10.1038/nrd.2016.175 (2016).  
717

718 **FIGURE CAPTIONS**

719

720 **Figure 1 | Overview of physiomimetic approach.** Our development of IPF disease-specific cell  
721 culture substrates is guided by a physiomimetic approach that aims to identify and isolate the  
722 human disease environment, then develop and investigate disease-specific ECM substrates *in*  
723 *vitro* utilizing disease-relevant human cell types (e.g., pulmonary fibroblasts) whose phenotype  
724 can be directly compared against diseased human IPF lung specimens prior to application in IPF  
725 disease models and antifibrotic drug testing.

726

727 **Figure 2 | Histological & biochemical characterization of ECM structural components in**  
728 **IPF lung tissues and matrix scaffolds.** Representative micrographs of histologic stains: (A)  
729 hematoxylin and eosin (H&E), (B) trichrome (collagens, blue), and (C) Verhoeff–Van Gieson  
730 (VVG, elastic fibers, black) demonstrating differences in histomorphology of IPF and normal lung  
731 tissues and scaffolds. Star indicates representative region with severe fibrosis and loss of elastic  
732 fibers. Quantification of structural ECM components (D) collagens and (E) elastin by biochemical  
733 assays. (F) Changes from normal lung in structural ECM components in IPF. H&E: hematoxylin  
734 and eosin, VVG: Verhoeff–Van Gieson.

735

736 **Figure 3 | Characterization of proteoglycans and glycoproteins in IPF lung tissues and**  
737 **matrix scaffolds.** Representative micrographs of histologic stains: (A) Alcian blue  
738 (proteoglycans, blue) and (B) pentachrome (acidic polysaccharides, green) demonstrating  
739 differences in proteoglycans between IPF and normal lung tissues. Arrow indicates normal airway  
740 epithelium. Quantification of sulfated glycosaminoglycan ECM components in (C) native tissues  
741 and (D) matrix scaffolds. (E) Changes from normal lung in glycosaminoglycan ECM components  
742 in IPF. Immunohistochemical staining of glycoprotein ECM components in IPF: (F) fibrillin 2, (G)



743 laminin  $\gamma 1$ , (H) matrix gla protein (MGP), (I) periostin. (J) Quantification of glycoproteins by image  
744 analysis of immunohistochemical staining using DensitoQuant software.

745

746 **Table 1 | Mass spectrometry analysis of IPF lung matrisome.** Changes from normal in  
747 the abundance of IPF lung matrisome components. PG: proteoglycan, BM: basement membrane.

748

749 **Table 2 | Quantification of growth factors in IPF and normal lung matrix scaffolds.** Growth  
750 factor concentrations were measured by multiplex growth factor array. Green arrow ( $\blacktriangle$ ) indicates  
751 positive fold change (increase) from normal in concentration of growth factors. Red arrow ( $\blacktriangledown$ )  
752 indicates negative fold change (decrease) from normal in concentration of growth factors. ND: not  
753 detected.

754

755 **Figure 4 | Structural, topographical, and mechanical characterization of IPF**  
756 **lung scaffolds.** Representative images of IPF and normal lung scaffolds: (A) gross photography,  
757 (B) scanning electron microscopy, (C) light microscopy (inverted color micrograph) of trichome  
758 staining demonstrating topography of ECM fibers in IPF scaffolds, (D) transmission electron  
759 microscopy. A: airspace, C: alveolar capillary, E: elastin bundle fragments, F: fibroconnective  
760 collagenous matrix, arrow: basement membrane. (E) Representative uniaxial stress-strain curves  
761 of IPF and normal lung tissues and matrix scaffolds. (F) Change in uniaxial mechanical stress  
762 from normal lung tissues and matrix scaffolds. (G) Tangent modulus values. Statistical analyses  
763 between tissues and scaffolds were performed using Student's *t*-test, with significance when  $p <$   
764 0.05. All values represent mean  $\pm$  standard deviation.

765

766 **Figure 5 | Phenotype of lung fibroblasts in IPF and normal lung scaffolds.** Representative  
767 micrographs of (A) H&E and immunohistochemical staining of (B) alpha smooth muscle actin  
768 ( $\alpha$ SMA) and (C) Forkhead box O3 (FOXO3). (D) Gene expression of normal human lung

769 fibroblasts cultured in IPF and normal lung scaffolds. \*  $p < 0.05$ , \*\*  $p < 0.01$ , ns:  
770 not significant. Quantification by ELISA of (E) basic fibroblast growth factor (bFGF, \*  $p < 0.05$ )  
771 and (F) transforming growth factor beta (TGF $\beta$ , \*  $p < 0.05$ ) secreted by normal human lung  
772 fibroblast cultured in IPF and normal lung scaffolds and on tissue culture plastic. All values  
773 represent mean  $\pm$  standard deviation.

774  
775 **Figure 6 | Demonstration of antifibrotic drug testing in IPF lung scaffolds.** (A) Growth curves  
776 of normal human lung fibroblasts over 6 days of treatment with PF3644022. (B) Gene expression  
777 of normal human lung fibroblasts cultured on IPF scaffolds and tissue culture plastic. \*  $p < 0.05$ ,  
778 \*\*  $p < 0.01$ . Quantification by ELISA of (C) basic fibroblast growth factor (bFGF,  $p = 0.0024$  by  
779 ANOVA) and (D) transforming growth factor beta (TGF $\beta$ ,  $p = 0.0084$  by ANOVA) secreted by  
780 normal lung fibroblast cultured in IPF and normal lung scaffolds and on tissue culture plastic. All  
781 values represent mean  $\pm$  standard deviation.

782  
783 **Supplementary Figure 1 | Characterization of human IPF and normal lung tissues.** (A)  
784 Donor characteristics of IPF and normal lung tissues. (B) Representative chest radiographs of  
785 IPF and normal lung donors. Arrows indicate changed lung shape, decreased lung volume,  
786 and increased radiopacity consistent with pulmonary fibrosis. (C) Fibrosis scoring rubric used to  
787 assess the extent of architectural disruption and fibrosis in human lung tissues. (D) Overview of  
788 the description and quantity of tissue samples analyzed in this study. Samples were collected  
789 from three regions (i.e., medial, lateral, peripheral) of right middle lobes. (F) Demonstration of  
790 quantitative image analysis method used for fibrosis scoring. For each fibrosis score, a weighted  
791 average is calculated from the ratios of the total area. Five high-power fields were analyzed per  
792 region, and an average fibrosis score was calculated for each region. (G) Fibrosis scores of  
793 all regions of IPF and normal lungs investigated in this study. Only regions of IPF lungs with  
794 fibrosis score  $\geq 2$  (red triangle) were investigated in this study. \*  $p < 0.001$ .

795 **Supplementary Figure 2 | Quality control assays of IPF and normal lung**  
796 **matrix scaffolds.** Quantification of (A) DNA to confirm removal of nuclear material from IPF  
797 and normal lung matrix scaffolds. (B) Results of sterility and mycoplasma assays. Prior to use in  
798 studies, IPF and normal lung matrix scaffolds were tested for absence of bacteria and fungi.  
799 Scaffolds were also tested for absence of mycoplasma using MycoAlert PLUS Mycoplasma  
800 Detection Assay. \*  $p < 0.001$ .

801

802 **Supplementary Table 1 | Antibodies and ELISA kits.**

803

804 **Supplementary Table 2 | Primers.**

805

806 **Supplementary Table 3 | Demographic and clinical characteristics of human lung donors.**

807 UIP, usual interstitial pneumonia.

808

809 **Supplementary Table 4 | Quantification of growth factors in IPF and normal lung tissues.**

810 Growth factor concentrations were measured by multiplex growth factor array. Green arrow (▲)  
811 indicates positive fold change (increase) from normal in concentration of growth factors. Red  
812 arrow (▼) indicates negative fold change (decrease) from normal in concentration of growth  
813 factors. ND: not detected. \* IPF-specific growth factor not detected in normal lung tissue.

814 **SUPPLEMENTARY INFORMATION**

815

816 **Characterization of human IPF and normal lung tissues.** Donor characteristics of IPF and  
817 normal lung tissues were analyzed to confirm that there were no significant differences in age,  
818 height, weight, body mass index, or smoking history (**Supplementary Fig. 1A, Supplementary**  
819 **Table 3**). The mean lung allocation score for IPF donors was  $55.0 \pm 25.1$ , which was the only  
820 significant difference between IPF and normal lung donors ( $p < 0.05$ ). Chest radiographs of lung  
821 donors confirmed absence of apparent injury or underlying disease in normal lungs, and enabled  
822 assessment of the extent and distribution of pulmonary fibrosis in IPF lungs. In contrast to normal  
823 lungs, which appeared radiolucent and aerated, IPF lungs displayed a morphologic pattern of  
824 usual interstitial pneumonia consistent with IPF and marked by diffuse radiopacities, reticulation,  
825 architectural distortion, and honeycombing, especially in peripheral and basal regions  
826 (**Supplementary Fig. 1B**).

827

828 In order to characterize the histopathology of all tissues investigated, a fibrosis scoring rubric was  
829 used to assess the extent of architectural disruption and fibrosis (**Supplementary Fig. 1C**).  
830 Samples were systematically collected from the medial and lateral regions of the right middle and  
831 right lower lobes. Histologic samples were evaluated by light microscopy, and fibrosis scores were  
832 assigned and averaged across five high-power fields. All high-power fields were subjected to  
833 imaging analyses to quantify the relative areas corresponding to each fibrosis score  
834 (**Supplementary Fig. 1F**). To ensure to the maximum possible extent a consistent degree of  
835 pulmonary fibrosis across all samples, only samples with average fibrosis score  $\geq 2$  (moderate or  
836 severe fibrosis) were investigated in this study (**Supplementary Fig. 1G**).

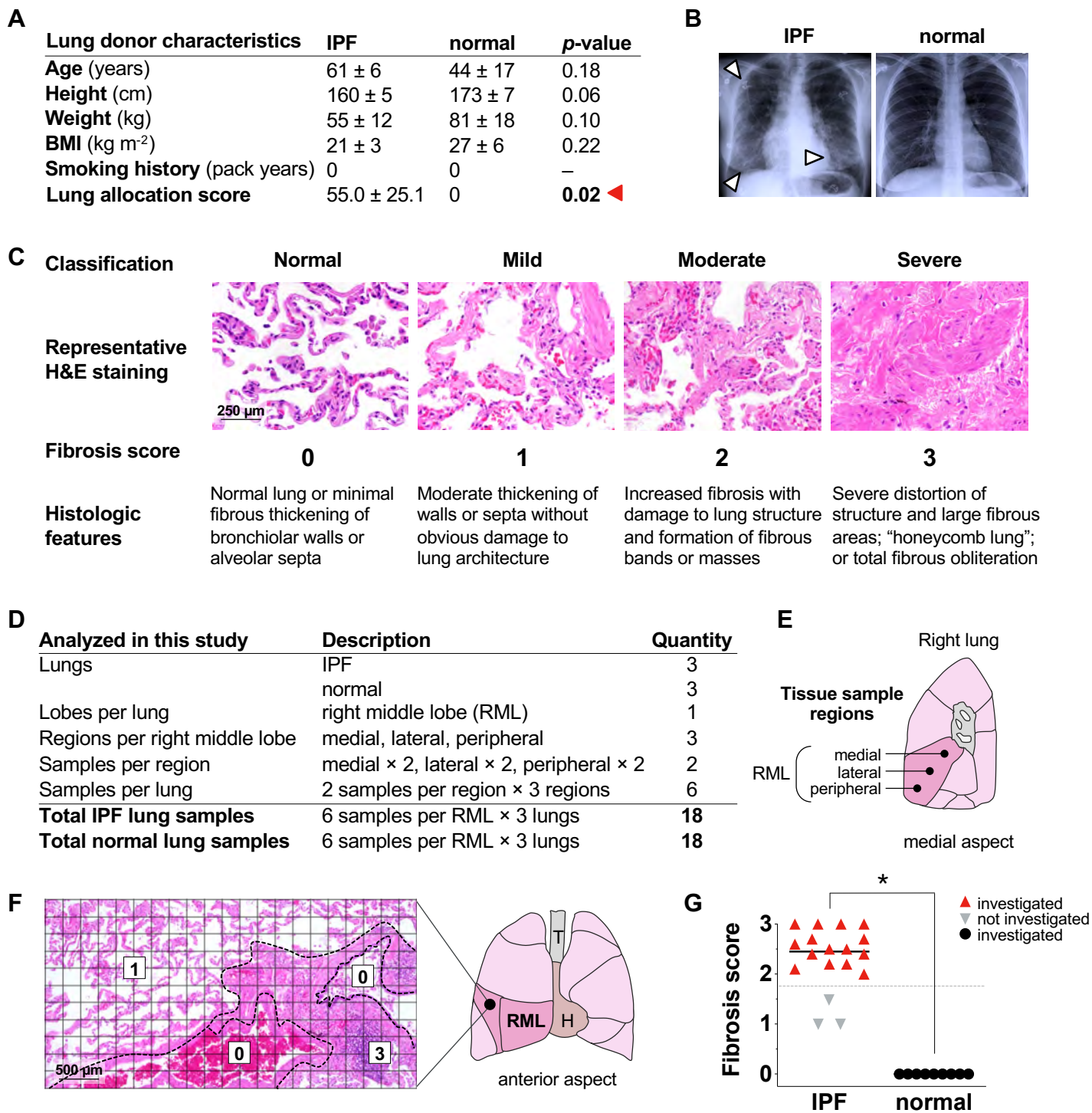
837

838 **Mass spectrometry.** Protein profiling included short gel SDS-PAGE, in-gel digestion with trypsin,  
839 and 2 hours LC-MS/MS. Samples were weighed and suspended in 130  $\mu\text{L}$  of 2.0% modified RIPA

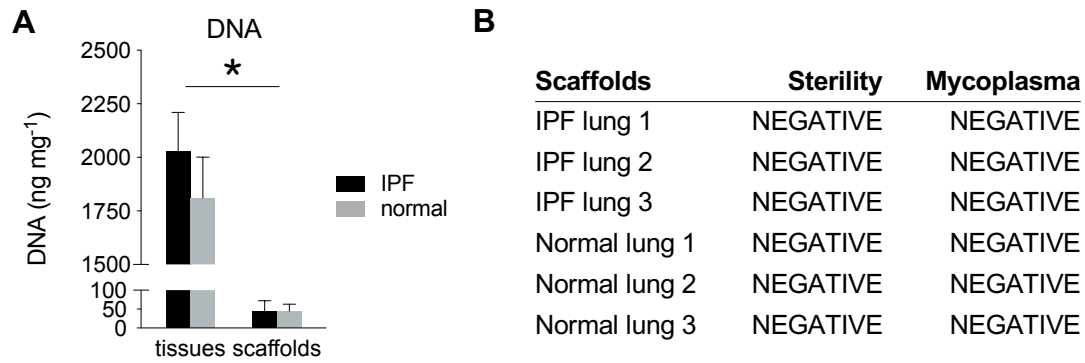
840 buffer with 1.6 mm stainless steel beads. Samples were homogenized in a Next Advance Bullet  
841 Blender for 3 minutes at speed 10, then heated at 100°C for 30 minutes. Samples were then  
842 sonicated and clarified by centrifugation. The protein concentration of the extract was determined  
843 using Qubit fluorometry (Life Technologies). Each sample (10 µg) was processed by 2 cm SDS-  
844 PAGE using a 10% Bis-Tris NuPAGE Novex mini gel (ThermoFisher) with the MES buffer system.  
845 The mobility region was excised and processed by in-gel digestion with trypsin using a ProGest  
846 robot (DigiLab) with the following protocol: (1) Wash with 25 mM ammonium bicarbonate followed  
847 by acetonitrile. (2) Reduce with 10 mM dithiothreitol at 60°C followed by alkylation with 50 mM  
848 iodoacetamide at room temperature. (3) Digest with sequencing grade trypsin (Promega) at 37°C  
849 for 4 hours. (4) Quench with formic acid and analyzed without further processing.

850

851 Half of each digest was analyzed by nano LC-MS/MS with a Waters NanoAcquity HPLC system  
852 interfaced to a mass spectrometer (Fusion Lumos, ThermoFisher). Peptides were loaded on a  
853 trapping column and eluted over a 75 µm analytical column at 350 nL min<sup>-1</sup> with a reverse phase  
854 gradient for 2 hours. Both columns were packed with Luna C18 resin (Phenomenex). The mass  
855 spectrometer was operated in data-dependent mode, with the Orbitrap operating at 60,000  
856 FWHM and 15,000 FWHM for MS and MS/MS, respectively. The instrument was run with a 3  
857 second cycle for MS and MS/MS. Advanced Precursor Determination was employed. Data were  
858 searched using a local copy of Mascot (Matrix Science) with the following parameters: Enzyme:  
859 Trypsin/P; Database: SwissProt Human (concatenated forward and reverse plus common  
860 contaminants); Fixed modification: Carbamidomethyl (C); Variable modifications: Oxidation (M/P),  
861 Acetyl (N-term), Pyro-Glu (N-term Q), Deamidation (N,Q); Mass values: Monoisotopic; Peptide  
862 Mass Tolerance: 10 ppm; Fragment Mass Tolerance: 0.02 Da; Max Missed Cleavages: 2. Mascot  
863 DAT files were parsed into Scaffold (Proteome software) for validation and filtering to create a  
864 non-redundant list per sample. Data were filtered using at least 1% protein and peptide FDR, and  
865 requiring at least two unique peptides per protein.



**Supplementary Figure 1 | Characterization of human IPF and normal lung tissues.** (A) Donor characteristics of IPF and normal lung tissues. (B) Representative chest radiographs of IPF and normal lung donors. Arrows indicate changed lung shape, decreased lung volume, and increased radiopacity consistent with pulmonary fibrosis. (C) Fibrosis scoring rubric used to assess the extent of architectural disruption and fibrosis in human lung tissues. (D) Overview of the description and quantity of tissue samples analyzed in this study. (E) Samples were collected from three regions (i.e., medial, lateral, peripheral) of right middle lobes. (F) Demonstration of quantitative image analysis method used for fibrosis scoring. For each fibrosis score, a weighted average is calculated from the ratios of the total area. Five high-power fields were analyzed per region, and an average fibrosis score was calculated for each region. (G) Fibrosis scores of all regions of IPF and normal lungs investigated in this study. Only regions of IPF lungs with fibrosis score  $\geq 2$  (red triangle) were investigated in this study. \*  $p < 0.001$ .



**Supplementary Figure 2 | Quality control assays of IPF and normal lung matrix scaffolds.** Quantification of **(A)** DNA to confirm removal of nuclear material from IPF and normal lung matrix scaffolds. **(B)** Results of sterility and mycoplasma assays. Prior to use in studies, IPF and normal lung matrix scaffolds were tested for absence of bacteria and fungi. Scaffolds were also tested for absence of mycoplasma using MycoAlert PLUS Mycoplasma Detection Assay. \*  $p < 0.001$ .

<b>Antibody</b>	<b>Application</b>	<b>Vendor</b>	<b>Product number</b>	<b>Dilution</b>
Rabbit anti-alpha smooth muscle actin	IHC-P	Cell Signaling Technology	19245	1 : 500
Rabbit anti-fibrillin 2	IHC-P	Sigma Life Science	HPA012853	1 : 50
Rabbit anti-Ki67	IHC-P	ThermoFisher Scientific	PA1-38032	1 : 500
Rabbit anti-laminin $\gamma$ 1	IHC-P	Abcam	ab233389	1 : 2000
Rabbit anti-matrix gla protein	IHC-P	LS Bio	LS-B14824	1 : 100
Rabbit anti-periostin	IHC-P	Abcam	ab14041	1 : 300

<b>ELISA kit</b>	<b>Application</b>	<b>Vendor</b>	<b>Product number</b>
Human basic fibroblast growth factor	Cell culture media	R&D Systems	DFB50
Human transforming growth factor $\beta$	Cell culture media	R&D Systems	DB100B

---

**Supplementary Table 1 | Antibodies and ELISA kits.**



<b>Gene</b>	<b>Forward primer</b>	<b>Reverse primer</b>
GAPDH	TGCACCACCAACTGCTTAGC	GGCATGGACTGTGGTCATGAG
MMP2	CTTCCAAGTCTGGAGCGATGT	TACCGTCAAAGGGGTATCCAT
COL1A1	TCTGCGACAACGGCAAGGTG	GACGCCGGTGGTTTCTTGGT
LAMC1	TGGGCATTCTTCTGTCTGTACAA	GCCACCCATCCTCATCAATC
ACTA2	CCTGGCTTCGCTGTCTACCT	TTGCGGTGGACGATGGA
PDGFC	GGA CTCAGGCGGAATCCAA	CTGAGGATCTTGTACTCCGTTCTG
YAP1	ACG TTCATCTGGGACAGCAT	GTTGGGAGATGGCAAAGACA
PRRX1	CAGATTGGTGGCTGTTAGATTGAA	GATGCACTTTTAGCACACATTTGTATT
PTEN	CAAGATGATGTTTGAAACTATTCCAATG	CCTTTAGCTGGCAGACCACAA

**Supplementary Table 2 | Primers.**

### IPF lung donor demographics and clinical characteristics

Characteristics	Donor 1	Donor 2	Donor 3
<b>Sex</b>	Female	Male	Female
<b>Age (years)</b>	62	66	55
<b>Height (cm)</b>	163	163	155
<b>Weight (kg)</b>	59	64	42
<b>BMI (kg m<sup>-2</sup>)</b>	22	24	18
<b>Smoking history (pack years)</b>	0	0	0
<b>Lung disease</b>	IPF	IPF	IPF
<b>Lung allocation score</b>	36.1	83.5	45.5
<b>Radiologic characteristics</b>	UIP, reticular opacities	UIP, honeycombing	UIP, reticular opacities

### NORMAL lung donor demographics and clinical characteristics

Characteristics	Donor 1	Donor 2	Donor 3
<b>Sex</b>	Female	Male	Male
<b>Age (years)</b>	24	56	52
<b>Height (cm)</b>	165	175	178
<b>Weight (kg)</b>	81	63	99
<b>BMI (kg m<sup>-2</sup>)</b>	30	20	31
<b>Smoking history (pack years)</b>	0	0	0
<b>Lung disease</b>	None	None	None
<b>Lung allocation score</b>	0	0	0
<b>Radiologic characteristics</b>	Abnormal basilar aeration	Cardiac enlargement	Trace pleural effusion

**Supplementary Table 3 | Demographics and clinical characteristics of human lung donors.** UIP, usual interstitial pneumonia.

Growth factor	Description	Concentration (pg mL <sup>-1</sup> )		Fold change from normal
		Normal tissue	IPF tissue	
TGF-β3	Transforming growth factor β3	ND	65.8	*
HB-EGF	Heparin-binding EGF-like growth factor	ND	4.2	*
IGFBP-1	Insulin-like growth factor binding protein 1	0.5	86.8	159.5 ▲
bFGF	Basic fibroblast growth factor	10.1	213.8	21.2 ▲
EG-VEGF	Endocrine gland-derived vascular endothelial growth factor	2.2	38.1	17.3 ▲
BDNF	Brain-derived neurotrophic factor	31.1	145.4	4.7 ▲
GDF-15	Growth differentiation factor 15	97.8	243.4	2.5 ▲
PDGF-AA	Platelet-derived growth factor AA	228.1	486.7	2.1 ▲
IGFBP-6	Insulin-like growth factor binding protein 6	123.0	228.5	1.9 ▲
HGF	Hepatocyte growth factor	13313.2	19831.9	1.5 ▲
VEGF	Vascular endothelial growth factor	135.9	158.8	1.2 ▲
EGF R	Epidermal growth factor receptor	17343.2	12828.8	0.7 ▼
OPG	Osteoprotegerin	60.8	33.8	0.6 ▼

**Supplementary Table 4 | Quantification of growth factors in IPF and normal lung tissues.** Growth factor concentrations were measured by multiplex growth factor array. Green arrow (▲) indicates positive fold change (increase) from normal in concentration of growth factors. Red arrow (▼) indicates negative fold change (decrease) from normal in concentration of growth factors. ND: not detected. \* IPF-specific growth factor not detected in normal lung tissue.